Selective autophagy regulates chloroplast protein import and promotes plant stress tolerance

Authors:

Chen Wan[1,2]#, Hui Zhang[1]#, Hongying Cheng[1,2], Robert G. Sowden[3], Wenjuan Cai[4], R. Paul Jarvis[3] and Qihua Ling[1,2,5]*

Affiliations:

[1] National Key Laboratory of Plant Molecular Genetics, CAS Centre for Excellence in Molecular Plant Sciences, Institute of Plant Physiology and Ecology, Shanghai Institutes for Biological Sciences, Chinese Academy of Sciences, Shanghai, China.

[2] University of Chinese Academy of Sciences, Beijing, China.

[3] Department of Plant Sciences, University of Oxford, Oxford OX1 3RB, UK.

[4] Core Facility Center, CAS Centre for Excellence in Molecular Plant Sciences, Chinese Academy of Sciences, Shanghai, China.

[5] CAS-JIC Center of Excellence for Plant and Microbial Sciences (CEPAMS), Institute of Plant Physiology and Ecology, Chinese Academy of Sciences, Shanghai, China.

*Correspondence to Qihua Ling (qhling@cemps.ac.cn).

# These authors contributed equally.

Abstract

Chloroplasts are plant organelles responsible for photosynthesis and environmental sensing. Most chloroplast proteins are imported from the cytosol through the translocon at the outer envelope membrane of chloroplasts (TOC). Previous work showed that TOC components are regulated by the ubiquitin-proteasome system (UPS) to control the chloroplast proteome, which is crucial for organellar functions and plant development. Here, we demonstrate that the TOC apparatus is also subject to K63-type polyubiquitination and regulation by selective autophagy, potentially to promote plant stress tolerance. We identify NBR1 as a selective autophagy adaptor targeting TOC components, and mediating their relocation into vacuoles for autophagic degradation. Such selective autophagy is shown to control TOC protein levels, and chloroplast protein import, and to influence photosynthetic activity and UVB and heat stress tolerance in *Arabidopsis* plants. The work first time reveals the vital role of selective autophagy in the proteolytic regulation of specific chloroplast proteins, and how dynamic control of chloroplast protein import is critically important for plants to cope with challenging environments.

Keywords

Chloroplast, NBR1, Autophagy, Protein import, Stress response

Introduction

Chloroplasts (and other plastids) are distinctive organelles in plants and algae which evolved through endosymbiosis from a cyanobacterial ancestor over one billion years ago (Jarvis & López-Juez, 2013). Chloroplasts are responsible for photosynthesis, arguably the most important biological process, which converts CO_2 into organic matter. By doing so, they not only provide a food source for life on Earth, but also release O_2 for respiration and control atmospheric CO_2 levels. In addition, chloroplasts have versatile functions, such as fatty acid and amino acid production and delivering responses to environmental cues (Rolland *et al*, 2012; Schwenkert *et al*, 2022). The establishment and maintenance of chloroplast functions are linked to the control of the organellar proteome.

The chloroplast proteome consists of about 3000 proteins. Although the chloroplast genome does encode some of these proteins, over 90% of chloroplast proteins are encoded in the nucleus. They are synthesized in the cytosol in precursor form, and thus must be imported into chloroplasts posttranslationally and processed, in order to take on their final conformation and functions (Li & Teng, 2013). Protein import is mediated by two multiprotein complexes in the outer and inner membranes, called TOC and TIC (Translocon at the Outer/Inner envelope membrane of Chloroplasts), respectively (Richardson *et al*, 2017; Rochaix, 2022; Shi & Theg, 2013). Protein import initiates at the TOC complex, which comprises three key components: two GTPase-domain receptors, Toc34 and Toc159, and one Omp85 (Outer membrane protein, 85 kD)-related membrane channel, Toc75 (Demarsy *et al*, 2014).

Accumulating evidence suggests that chloroplast protein import is not a constitutive process, but, instead, can be rapidly regulated by the ubiquitin-proteasome system (UPS). Such regulation is crucial to chloroplast biogenesis and operation in response to developmental and environmental cues (Ling & Jarvis, 2015a). The UPS is a major eukaryotic protein degradation system that implements the ubiquitin signal to turnover specific target proteins (Vierstra, 2009). Genetic analysis revealed that TOC components can be directly targeted for degradation by the proteasome, mediated by a chloroplast-localized ubiquitin E3 ligase, SP1 (Ling *et al*, 2012). Recently, SP1 was shown to act in a novel pathway controlling chloroplast protein stability, named chloroplast-associated protein degradation (CHLORAD) (Ling *et al*, 2019). CHLORAD regulates protein import to optimize the organellar proteome, and is thereby important for the interconversions that chloroplasts and other plastid types undergo (for example, during de-etiolation and fruit ripening) (Ling *et al.*, 2012; Ling *et al*, 2021), and for abiotic stress tolerance (Ling & Jarvis, 2015b). Apart from CHLORAD, cytosolic ubiquitin-dependent systems can also govern protein import, by regulating precursor stability (Grimmer *et al*, 2020; Lee *et al*, 2009), or by controlling the abundance of the Toc159 receptor before its entrance into the outer envelope membrane (Shanmugabalaji *et al*, 2018).

Autophagy is another conserved eukaryotic proteolytic pathway, and it is critical for responses to various forms of stress, such as nutrient deprivation or abiotic stress (Avila-Ospina *et al*, 2014; Chen *et al*, 2021; Marshall & Vierstra, 2018). Cargos to be degraded by autophagy are sequestered into double-membrane vesicles called autophagosomes, and then delivered to lysosomes or vacuoles as autophagic bodies for recycling. Autophagy-related (ATG) proteins are essential for the formation of autophagosomes (Nakatogawa, 2020). Although autophagy was long thought to be responsible for non-selective bulk degradation, it is clear now that autophagy can selectively eliminate unwanted or damaged proteins or organelles (Dikic & Elazar, 2018; Nakamura *et al*, 2021; Palikaras *et al*, 2018; Stephani & Dagdas, 2020). The most prevalent selective autophagy pathway requires the labelling of the substrate with specific signals (such as ubiquitin) that are recognized by autophagy adaptors, which guide the cargo to the autophagic

membrane via their ATG8-interaction motif (AIM) or ubiquitin-interacting motif (UIM) (Kirkin & Rogov, 2019).

Compared with organelles in yeast and mammals, chloroplasts have been studied to a much lesser extent regarding autophagy. Given that they are unique to plants and algae, distinctive autophagy pathway components are expected to operate in chloroplasts. Two main types of chloroplast autophagy (or called chlorophagy) have been revealed: bulk degradation of Rubisco-containing bodies during dark-induced senescence (Ishida *et al*, 2008; Wada *et al*, 2009), and degradation of whole photodamaged chloroplasts (Izumi *et al*, 2017; Nakamura *et al*, 2018). However, little is known about the roles of selective autophagy in regulating chloroplast proteins (Otegui, 2018), and selective chlorophagy receptors or adaptors have not been identified (Kirkin & Rogov, 2019; Wan & Ling, 2022), with the exception of ATI1, a potential receptor for chloroplast degradation (Avin-Wittenberg *et al*, 2012; Michaeli *et al*, 2014). Moreover, the role of chloroplast autophagy in various abiotic stress, such as heat and UVB, is poorly understood.

To improve understanding of the ubiquitin-dependent proteolytic pathways acting on chloroplasts, here we analyzed the effect of autophagy impairment on the stability of specific chloroplast proteins. We showed that protein import is regulated through selective degradation of TOC components by autophagy, in a process that is distinct from CHLORAD. We identified a selective autophagy adaptor, NBR1, and demonstrated that NBR1 mediates the degradation of the TOC complex in response to heat and UVB stresses. Collectively, our results reveal a novel mechanism of chloroplast protein quality control involving selective autophagy.

Results

TOC components are degraded by autophagy pathway

Although chloroplasts were discovered as the target of autophagy more than a decade ago, the molecular mechanisms that govern this process have largely remained elusive. It is known that protein ubiquitination serves not only as a targeting signal for the UPS, but also as a targeting signal for selective autophagy pathways (Kwon & Ciechanover, 2017). Our previous finding that TOC components can be ubiquitinated suggests a possible signal for the selective autophagy of chloroplast proteins. To shed light in this area, we performed a series of cellular, molecular and biochemical analyses.

First, to determine whether TOC components are autophagy cargo proteins, we transiently expressed yellow fluorescent protein (YFP)-tagged Toc33, Toc159 and Toc75 in Arabidopsis protoplasts. The YFP tag was fused to Toc33 and Toc159 at their N termini, and inserted in-between the transit peptide and the N terminus of the Toc75 mature sequence (Chen *et al*, 2016; Paila *et al*, 2016), so as not to interfere with proper membrane integration. In parallel, SP1-YFP and FAX1 (fatty acid export 1)-YFP were expressed in protoplasts as control proteins; FAX1 is a chloroplast envelope protein involved in fatty acid metabolism. Both SP1 and FAX1 are CHLORAD substrates like TOC proteins (Sun *et al*, 2022), and previously we demonstrated that SP1 is not subjected to autophagic degradation (Ling *et al.*, 2019). Protoplasts expressing all constructs were treated with concanamycin A (ConA), an inhibitor of tonoplast H^+-ATPase that blocks vacuolar proteolysis by increasing luminal pH (Nolan *et al*, 2017). As protoplastation and transfection cause abiotic stress (Ling & Jarvis, 2015b), autophagy is expected to be induced under such conditions. Indeed, treatment of cells expressing YFP-tagged TOC proteins with ConA resulted in the accumulation of randomly moving YFP-labelled puncta, which we interpret to be vacuolar autophagic

bodies, in addition to the signals at chloroplasts; whereas treatment of cells expressing SP1-YFP and FAX1-YFP exhibited only signals around the chloroplasts (Fig 1A and B; Movie EV1). In the absence of ConA treatment, vacuolar YFP puncta were largely absent for all constructs (Fig EV1), supporting our interpretation of autophagic degradation of TOC proteins in the vacuole. As the YFP-labelled puncta are similar or even smaller in size than typical autophagosomes, we infer that TOC proteins are most likely degraded by a macroautophagy pathway (Nakamura *et al.*, 2018). To further confirm that TOC proteins are degraded by autophagy, we coexpressed YFP-Toc33, YFP-Toc159 or YFP-Toc75 together with the autophagosome marker CFP-ATG8 (ATG8a) in protoplasts, with ConA treatment. Confocal microscopy analyses demonstrated that ATG8 (blue puncta) and TOC proteins (green puncta) co-localized in the vacuole (Fig 1C; Movie EV2), suggesting that turnover of TOC proteins is indeed associated with ATG8-decorated autophagic particles.

To verify the above results, we also generated stable transgenic lines expressing YFP-Toc33 (*pToc33:YFP-Toc33*) and YFP-Toc75 (*pToc75:YFP-Toc75*) fusions under the control of the respective native promoters. By quantifying the accumulation of YFP-Toc33 and YFP-Toc75 in the transgenic lines, we showed that the levels of these YFP-tagged proteins are similar to those of the endogenous proteins (Appendix Fig S1A-D). Both lines were grown in the dark with ConA treatment for two days to induce autophagy. In both cases, the accumulation of YFP-labelled puncta in the vacuole was evident, confirming the turnover of TOC proteins in the vacuole (Fig 1D, Appendix Fig S2A and B, and Movie EV3). To directly determine whether the detection of YFP-TOC puncta was linked to autophagy, we generated Arabidopsis *atg7-2* autophagy mutant plants that stably express the *pToc33:YFP-Toc33* or *pToc75:YFP-Toc75* transgenes. ATG7 is the E1 enzyme for ATG8 activation, and the *atg7* mutant was reported to compromise the process of autophagosome formation (Shin *et al*, 2014; Spitzer *et al*, 2015). In the *atg7-2* mutant, treated as described for Fig 1D, no obvious YFP-labelled puncta could be observed in the vacuole (Figs 2A and EV2), consistent with the notion that TOC proteins were autophagic cargos.

We next analyzed native TOC protein levels in wild-type and *atg7-2* plants, grown in the dark and treated with or without bortezomib (a proteasome inhibitor) or E64d (a cysteine protease inhibitor, which allows us to check accumulation of autophagic cargo in the vacuole, like ConA) (Ling *et al.*, 2019; Nolan *et al.*, 2017). As expected, accumulation of all main TOC proteins was significantly elevated after bortezomib treatment (Student's *t* test, $P < 0.05$), since they are known UPS substrates (Ling *et al.*, 2012) (Fig 2B and C). Notably, TOC protein levels were similarly increased after E64d treatment, or in the *atg7* mutant compared with the wild-type plants (Fig 2B and C). In contrast, a component of the TIC complex, Tic110, was stable in both genotypes and under all treatments, suggesting that TOC proteins are selective autophagy cargos. The influence of autophagy on TOC proteins was further confirmed by ConA treatment, which had a similar effect to E64d (Appendix Fig S3A and B). In the *atg7-2* background or after E64d treatment, even higher TOC protein levels could be detected after bortezomib treatment, whereas the additivity of increased TOC protein levels was absent in *atg7-2* mutant treated with E64d (Fig 2B and C and Appendix Fig S3A and B), supporting the notion that the UPS and autophagy are complementary pathways controlling TOC components. These changes were not attributable to regulation at the mRNA level, because TOC transcript levels were comparable in the different genotypes and treatments (Appendix Fig S4A and B).

Identification of NBR1 as an autophagic adaptor for chloroplasts

To shed light on the molecular mechanism for the recognition of chloroplast cargos in selective autophagy,

we sought receptors or adaptors of chloroplast proteins by screening for ATG8 interactors in chloroplasts. We first checked the proportion of cellular ATG8 protein localized in chloroplasts. Constructs encoding YFP-ATG8 or free YFP were transiently expressed in Arabidopsis protoplasts for confocal microscopy analysis. In contrast to free YFP, which only showed diffuse cytosolic localization, YFP-ATG8 also presented puncta around the periphery of chloroplasts in a pattern indicative of envelope localization (Fig 3A, upper panels). Chloroplast localization of YFP-ATG8 was clearer when the organelles were isolated from the protoplasts, whereas free YFP did not show such localization (Fig 3A, lower panels). To confirm the association of ATG8 with chloroplasts, the purified organelles, as well as their corresponding protoplasts were analyzed by immunoblotting (Fig 3B). By comparing with the Tic110 control protein that is exclusively localized in chloroplasts (Bédard *et al*, 2007; Ling *et al.*, 2012), we estimated a large proportion of ATG8 interacted with chloroplasts, whereas the control free YFP protein was only marginally associated with chloroplasts (Fig 3C). Similar results were obtained when chloroplast-associated ATG8 was detected using an ATG8 antibody (Appendix Fig S5A and B). These results implied that autophagy affects the chloroplast's proteins and functions extensively.

We then performed co-immunoprecipitation (co-IP) using YFP-Trap magnetic beads followed by mass spectrometry, using protein extracts prepared from the chloroplast fraction of cells expressing YFP-ATG8 or YFP-HA (Fig 3D). Using purified chloroplasts allowed us to focus on chloroplast ATG8 interactors, and to avoid detecting autophagy cargos in other organelles, because ATG8 is an abundant cellular constituent distributed throughout the nucleocytosolic compartment. After normalization and excluding proteins bound non-specifically with YFP-HA, 150 proteins were identified as putative ATG8-interacting proteins associated with chloroplasts (Fig 3E and Dataset EV1). The candidate list included chloroplast proteins belonged to various functional categories, and they are localized in different suborganellar compartments, which could potentially be cargo proteins. As expected, TOC components were detected as interactors of ATG8, further confirming that they are autophagic cargos. In addition, among the list was NBR1 (Next to BRCA1 gene 1), a plant homologue of the mammalian autophagic cargo adaptor SQSTM1/p62 (Svenning *et al*, 2011). Considering the crucial role of p62 in mammals, it is surprising that Arabidopsis *nbr1* mutants do not show obvious defects under normal growth conditions (Zhou *et al*, 2013). Recently, NBR1 was reported to be responsible for selective autophagy in plants under stress conditions (Ji *et al*, 2020; Thirumalaikumar *et al*, 2021). However, the role of NBR1 in the selective autophagy of chloroplasts, if any, is unknown.

To assess whether NBR1 acts as an autophagy adaptor for chloroplast proteins, we first examined the association of NBR1 with chloroplasts in cells expressing NBR1-YFP. Confocal microscopy analysis demonstrated strong accumulation of YFP-labelled puncta in the cytosol, adjacent to chloroplast envelope where the TOC apparatus resides (Fig 3F, upper panel). The association of NBR1-YFP with chloroplasts became clear when the organelles were isolated from the cells (Fig 3F, lower panel). Such NBR1-chloroplast association was further verified by immunoblotting analysis of isolated chloroplast fractionations, which indicated that a considerable proportion of NBR1 is localized in the chloroplast (Fig 3G and H and Appendix Fig S5A and B). Collectively, these data implied that chloroplast proteins, particularly those localized at the envelope membrane, are likely selectively targeted by NBR1 for autophagic degradation.

NBR1 associates with TOC components

To test whether NBR1 is an adaptor for the selective autophagic degradation of TOC proteins, we first assessed co-localization using protoplasts coexpressing YFP-TOC protein fusions and NBR1-CFP. While TOC fusion proteins still produced a typical distributed signal at the periphery of the chloroplasts, similar to

when they are expressed alone (Bae et al, 2008) (Fig EV1 and Appendix Fig S6), all three TOC proteins (green puncta) also partially co-localized with NBR1 (blue puncta) at chloroplasts, in a similar punctate pattern to NBR1 alone (Fig 4A, Fig 3F and Appendix Fig S6). In contrast, the control fusion proteins SP1-YFP and FAX1-YFP displayed only distributed (non-punctate) chloroplast envelope fluorescence, even when coexpressed with NBR1-CFP (Fig 4A). Chloroplast colocalization of NBR1-CFP with TOC-YFP fusion proteins was clearer when the organelles were isolated from the protoplasts, whereas SP1-YFP and FAX1-YFP did not show such colocalization with NBR1-CFP (Appendix Fig S7). These results suggest that NBR1 is able to recruit TOC proteins specifically. To further monitor co-localization in the vacuole, we also generated transgenic lines coexpressing mScarlet-tagged NBR1 and the YFP-tagged TOC proteins (i.e., *p35S:NBR1-mScarlet/pToc33:YFP-Toc33* and *p35S:NBR1-mScarlet/pToc75:YFP-Toc75*), by crossing. Plants were grown in the dark for two days with ConA treatment in order to induce autophagy and enhance the vacuolar fluorescence signals. As shown in Fig 4B and Movie EV4, the TOC (green) and NBR1 (red) signals co-localized in randomly moving vacuolar puncta that were most likely autophagic bodies. Such vacuolar puncta are similar in size to the ATG8-TOC puncta in Figure 1D, but appear smaller than the Rubisco-containing bodies (RCBs) described previously (Ishida *et al.*, 2008; Wada *et al.*, 2009), implying that they may contain distinct chloroplast cargos. While RCBs are known to contain various stromal proteins, we propose that the TOC-containing puncta contain mainly TOC complexes, although we cannot rule out the possibility that there might be other chloroplast proteins in the TOC-containing puncta.

To determine whether NBR1 interacts with the TOC complex, we carried out bimolecular fluorescence complementation (BiFC) experiments in Arabidopsis protoplasts. The NBR1 coding sequence was cloned into a vector that C-terminally appends the C-terminal half of YFP (cYFP); and a negative control construct encoding CDKA1, a cytosolic protein, was similarly generated. These cYFP constructs were coexpressed with various other constructs encoding the core TOC components (Toc33, Toc159 and Toc75) bearing the complementary, N-terminal moiety of the YFP protein (nYFP); or with a negative control construct encoding OEP7, a non-TOC outer envelope membrane protein, bearing the nYFP moiety appended C-terminally. This method can report on protein-protein interactions via the detection of YFP fluorescence, caused by reconstitution of functional YFP from the nYFP and cYFP fragments. Remarkably, NBR1 was found to physically associate with all tested TOC proteins, whereas CDKA1 barely interacted with the TOC proteins (Fig 4C and D). Moreover, these interactions displayed a punctate pattern adjacent to the chloroplast, placing them in an ideal subcellular context for the in situ regulation of the chloroplast protein import machinery by the cytosolic autophagy components. Conversely, OEP7-nYFP could not restore a fluorescence signal with NBR1-cYFP, suggesting selective targeting of the TOC apparatus by NBR1.

To verify the interactions, we employed co-IP assays, which were conducted using transgenic Arabidopsis plants stably expressing HA-tagged NBR1. In these experiments, NBR1-HA was enriched using anti-HA magnetic beads, and all of the core TOC components were detected in the fractions that co-eluted with NBR1-HA, using antibodies against the native proteins, but not in control elutions (Fig 4E). The specificity of these TOC component interactions was demonstrated by the absence of a control protein, Tic40, from the eluted fractions. Thus, we concluded that NBR1 may regulate TOC proteins directly.

NBR1 mediates autophagic degradation of TOC complex during UVB stress

Previously we showed that the TOC apparatus is controlled by SP1-dependent UPS action, in response to abiotic stresses such as salt and osmotic stresses (Ling & Jarvis, 2015b). Intriguingly, although chloroplast functions are apparently crucial under light and temperature stresses (Schwenkert *et al.*, 2022), no obvious

effect of SP1 was observed in these conditions, implying the involvement of alternative or complementary pathways (Ling & Jarvis, 2015b). The finding that NBR1 controls the TOC complex motivated us to investigate whether NBR1-mediated selective autophagy is responsible for the chloroplast responses to light and temperature stresses. Thus, we grew *atg7-2* and *nbr1-2* mutant and NBR1 overexpressor (NBR1-OX) Arabidopsis plants under abiotic stress conditions, starting with ultraviolet-B (UVB) treatment (5 $\mu E/m^2/s$) to mimic natural high light stress (Shi & Liu, 2021). Both *atg7* and *nbr1* mutant plants failed to cope with these conditions, whereas NBR1-OX plants were more stress tolerant than wild type, as judged by plant size and chlorophyll content (Fig 5A and B).

To understand the molecular basis for stress tolerance mediated by NBR1, we began by examining the levels of various chloroplast proteins in *atg7-2*, *nbr1-2* and NBR1-OX plants by immunoblotting, under UVB stress conditions, as the primary function of selective autophagy is to control protein abundance. For this work, we focused on short-term UVB stress (eight-day-old seedlings were exposed to UVB for 3 h, and then recovered under normal condition for 1 d), to avoid strong morphological changes that might lead to pleiotropic consequences, and to aid identification of the primary effects of the stress. The results revealed that protein abundance of TOC components declines significantly ($P < 0.05$) 1 d after the UVB treatment in the wild type, although no obvious effect was detected immediately after the UVB exposure (Fig 5C and D). This response was NBR1 and autophagy dependent, as it did not occur in the *atg7* and *nbr1* mutants; whereas the TOC proteins reached even lower levels in NBR1-OX plants. In contrast with the TOC proteins, a component of TIC apparatus did not change in abundance in response to the stress (Fig 5C and D). In addition, inspection of the protein banding pattern upon Coomassie staining revealed that the effect on TOC proteins was unlikely to be a general, damage-related phenomenon affecting many proteins (Fig 5C). Semi-quantitative RT-PCR analyses did not reveal significant changes in TOC transcript levels under the conditions employed, ruling out the possibility that the NBR1/autophagy-dependent changes of TOC protein levels were an indirect consequence of transcriptional effects (Appendix Fig S8).

NBR1 typically recognizes ubiquitinated cargo proteins (Sun *et al*, 2021b; Svenning *et al.*, 2011). To investigate whether ubiquitination of TOC proteins occurs in response to UVB stress, to stimulate selective autophagy, we assessed the ubiquitination status of the TOC components in vivo, with or without UVB treatment. Although polyubiquitination has the potential to trigger protein degradation through either the UPS or autophagy, distinct degradation signals involving specific linkage types within the ubiquitin chains are typically involved. For example, K48-linked polyubiquitin typically induces proteasomal proteolysis, whereas K63-linked chains can facilitate the autophagic degradation of protein substrates (Kwon & Ciechanover, 2017). Although TOC proteins are known targets of ubiquitination, the type of ubiquitin chain is unknown. To elucidate this, we purified Toc159 by immunoprecipitation using anti-Toc159 antibody (and the preimmune serum as a negative control) from wild-type Arabidopsis plants subjected to UVB exposure (alongside control plants), and the samples were subsequently analyzed by immunoblotting. Remarkably, high-molecular-weight smears were clearly visible in the precipitates of Toc159 protein, in blots using two linkage-specific ubiquitin antibodies, indicating that Toc159 is polyubiquitinated via both K48 and K63 linkages (Fig 5E). Moreover, not only the amount of detectable K48 ubiquitination, but also that of K63 ubiquitination, was dramatically enhanced when the plants were exposed to UVB stress (Fig 5 E and F). In contrast, Tic40, serving as a negative control, was not detected in the Toc159 precipitates. These results provided further strong support for the conclusion that chloroplast proteins are selectively regulated by ubiquitination and autophagy. Elevated K63 polyubiquitination of Toc159 upon UVB stress suggested that ubiquitination is involved in activating the autophagic degradation of TOC components.

In mammal, evidences indicate that NBR1 binds ubiquitinated proteins through its C-terminal UBA domains (Kirkin & Rogov, 2019). To assess whether the ubiquitination of TOC components is a prerequisite for their recruitment by NBR1, we employed co-IP assay using an NBR1-ΔUBA (deletion of both UBA domains) variant. As shown in Fig 4E, NBR1-ΔUBA resulted in strongly reduced binding with all three TOC protein, compared with full-length NBR1, indicating that the interaction between NBR1 and TOC substrates depends on ubiquitination.

As NBR1 was shown to bind both ATG8 and TOC proteins, we hypothesized that NBR1 serves as an intermediary between ATG8 and TOC proteins in selective autophagic degradation. To test this hypothesis, we employed co-IP assays, which were conducted using wild-type, *nbr1-2* mutant, and NBR1-OX Arabidopsis protoplasts expressing YFP-tagged ATG8. In these experiments, the interactions between YFP-ATG8 and TOC proteins were strongly increased by NBR1 overexpression, but largely diminished in *nbr1-2* mutant (Appendix Fig S9). These results suggest that NBR1 is responsible for the recruitment of ATG8 to TOC proteins for degradation.

NBR1 mediates autophagic degradation of TOC complex during heat stress

Temperature stress was reported to impair chloroplast protein import, through an unknown mechanism (Dutta *et al*, 2009). Thus, we next turned our attention to heat stress. In this case, we incubated soil-grown wild-type, *atg7-2*, *nbr1-2* and NBR1-OX mature Arabidopsis plants under 42°C for 17 h and then returned them to the normal growth conditions (22°C) for 2 d before their visible phenotypes were observed. Paralleling the UVB stress results, *atg7* and *nbr1* mutants failed to develop under these conditions, and exhibited severe leaf death, whereas NBR1 overexpressors were more stress tolerant than wild type, showing much bigger shoot size (Fig 6A).

As in the previous experiment, immunoblotting was performed to investigate the effect of short-term heat stress on TOC proteins of in vitro grown seedlings, and the results were essentially identical to those obtained for UVB stress: the TOC apparatus was specifically and quickly depleted under stress conditions, through the action of NBR1-mediated autophagy; whereas a TIC component and a chloroplast interior protein, AtpA, remained stable in response to stress (Fig 6B and C). Notably, such short-term heat stress did not cause obvious growth defect in the seedlings of all tested genotypes, ruling out the possibility that the changes of TOC protein levels were merely consequences of developmental abnormality. Differences in the abundance of the TOC proteins between genotypes and conditions were not linked to transcriptional changes between the genotypes, as the mRNA levels of the corresponding proteins were similar, as revealed by semi-quantitative RT-PCR (Appendix Fig S10). Collectively, our results indicate an important role for selective autophagy of chloroplast proteins in plant responses to UVB and heat stresses.

Degradation of TOC components mediated by NBR1 impacts protein import

We previously reported that SP1 acts to degrade the TOC apparatus under certain abiotic stresses to limit protein import (Ling & Jarvis, 2015b). To test whether altered NBR1 expression, and corresponding TOC protein level changes, can also influence chloroplast protein import efficiency, we first compared the import capabilities in vitro of chloroplasts purified from unstressed wild-type, *nbr1-2* mutant, and NBR1 overexpressor plants. Isolated chloroplasts were incubated with the precursor of the Rubisco small subunit (SSU), and import efficiency was assessed by quantifying the amount of mature, processed proteins in the organelles (Fig 7A). In this analysis, *nbr1* mutant chloroplasts displayed slightly elevated import efficiency of SSU, relative to wild type, whereas NBR1 overexpressor chloroplasts tended to show a decline in import

capacity (Fig 7A).

These data suggested that NBR1 may play a nuanced role in optimizing chloroplast protein import when plants are grown under normal conditions. However, changes of NBR1 expression had strong effects on TOC levels in plants grown under stress conditions (Fig 5D), implying that NBR1-mediated regulation of protein import may be especially important during stress. We attempted similar in vitro protein import assays using plants kept under stress conditions, but chloroplasts isolated from these plants proved to be incompetent for such assays, possibly due to fragility caused by stress damage. Thus, we conducted in vivo import experiments based on fluorescence recovery after photobleaching (FRAP) assay. For this purpose, we first introduced a chloroplast-targeted marker protein, cpGFP (Ishida *et al.*, 2008) into the wild-type, *nbr1-2*, *plastid protein import 1 (ppi1)* mutant, and NBR1-OX plants by crossing. The *ppi1* mutant is a knockout of Toc33 in which TOC activity is constitutively impaired, due to the permanent loss of Toc33 (Jarvis *et al*, 1998). The cpGFP marker is a GFP protein harbouring a chloroplast transit peptide, which is stably expressed in plants driven by the constitutive *35S* promoter. The chloroplast transit peptide enables cpGFP to be exclusively localized within the chloroplast stroma. In the FRAP assay, the chloroplast GFP signal in a cell was partially depleted by photobleaching using the confocal scanning laser microscope, enabling newly imported GFP molecules to be monitored as fluorescence signal recovery, due to new chromophore formation (Craggs, 2009). Thus, even when the plants were grown under stress conditions, it was possible to conduct non-destructive in situ assessments of relative chloroplast protein import efficiency from different genotypes.

When plants were grown under normal conditions, no clear differences in chloroplast import efficiency could be observed in *nbr1-2* and NBR1-OX leaves, as estimated by signal recovery (Fig 7B). By contrast, following exposure to UVB treatment, protein import was greatly enhanced in the *nbr1* mutant and dramatically reduced in NBR1-OX plants, compared with that in wild type (Fig 7C and Appendix Fig S11; Movie EV5 and EV6). In fact, stressed NBR1 overexpressors showed a defect in protein import comparable to that seen in *ppi1*. This implies that NBR1 is a strong regulator of protein import under stress conditions. Significantly, mutant and overexpressor plants displayed no obvious growth defects after the short-term UVB stress employed here. Thus, protein import was indeed specifically regulated by selective autophagy in response to stress, and not indirectly influenced as a result of growth differences between the genotypes under such conditions.

Altered NBR1 expression affects chloroplast morphology and photosynthesis

Protein import is essential for chloroplast biogenesis and maintenance (Jarvis & López-Juez, 2013). Plants with compromised protein import typically exhibit defective chloroplast morphology, with regard to chloroplast size and shape and thylakoid membrane structure (Bauer *et al*, 2000; Jarvis *et al.*, 1998; Kovacheva *et al*, 2005). We hypothesized that NBR1's role under stress is to quench chloroplast function by suppressing protein import. To test this possibility, we first analyzed chloroplast ultrastructure by transmission electron microscopy in *nbr1-2* and NBR1-OX plants, either kept under normal conditions or treated with short-term UVB stress. Although chloroplasts of *nbr1* mutant and NBR1 overexpressor plants had chloroplast morphology similar to the wild type in the absence of stress (Fig 7D), consistent with our earlier finding that altered NBR1 levels have minor consequences under such conditions, the importance of NBR1 was clearly revealed following stress treatment (Fig 7E). Strikingly, NBR1-OX chloroplasts were frequently deformed in shape, as illustrated by the decreased length/width ratio of the organelles (Fig 7F). In addition, they had severely disrupted thylakoid networks, as indicated by the significantly reduction in

thylakoid stacking compared with the wild type (Fig 7G). Moreover, after the UVB exposure, the number of starch granules in NBR1-OX chloroplasts was significantly decreased compared with the wild type (Fig 7H), suggesting lower carbon fixation efficiency. On the contrary, *nbr1* mutant chloroplasts appeared to respond even less to the UVB stress than wild type, regarding thylakoid complexity and starch granule number of the organelles.

Abundances of TOC proteins, such as Toc159 are dramatically reduced in *ppi1* mutant, and mutations of CHLORAD components, SP1 or SP2 can partially suppress the *ppi1* phenotype, possibly due to the increase of other TOC protein levels (Ling *et al.*, 2019; Ling *et al.*, 2012). To confirm the role of NBR1 in protein import genetically, we crossed *nbr1-2* mutant with *ppi1*, and phenotypically characterized the resultant double mutant. Intriguingly, it appeared greener than the *ppi1* single mutant, although *nbr1* single mutant was indistinguishable from the wild type (Fig 8A). Correspondingly, the leaf chlorophyll concentration of *nbr1 ppi1* was also significantly increased relative to *ppi1* (Fig 8B). To assess whether the phenotypic suppression observed in *ppi1 nbr1* was linked to changes in the abundance of TOC proteins, we analyzed the double mutant and control plants via immunoblotting. The double mutant displayed a clear increase in the abundance of Toc159 compared with *ppi1* (Fig 8C and D); note that possible effects of *nbr1* on Toc33 could not be assessed due to the complete inactivation of the *TOC33* gene in *ppi1*. These results indicated a genetic link between NBR1 and the chloroplast protein import apparatus.

To assess whether the aforementioned chloroplast morphology changes are linked to the role of NBR1 in TOC regulation, we also analyzed chloroplast ultrastructure in *ppi1* and *ppi1 nbr1-2* mutants under normal growth conditions. Although chloroplast size in these two mutants was not significantly different, the addition of the *nbr1* mutation partially recovered the defect of *ppi1* in thylakoid stacking (Fig 8E-G). These results support the hypothesis that TOC regulation by NBR1 influences chloroplast morphology.

Such NBR1-dependent changes of chloroplast morphology suggested that autophagic regulation of protein import plays an important role in adapting chloroplast functions (e.g., photosynthesis) in response to stress. To address this hypothesis, we assessed photosynthetic performance in these plants by measuring the parameter F_v/F_m, which represents the maximal quantum yield of PSII (Ling *et al.*, 2021). In line with the chloroplast morphology data, plants with altered NBR1 expression levels did not show obvious changes in the F_v/F_m value under the normal conditions used (Appendix Fig S12A). However, under UVB stress conditions, NBR1-OX plants showed clearly reduced F_v/F_m values (Appendix Fig S12B), suggesting that NBR1 acts to limit photosynthetic activity in response to stress. The abundancies of photosynthetic apparatus components PsaD and PsbP (both of which are imported into chloroplasts by the TOC apparatus) also declined markedly in the NBR1-OX plants under UVB stress conditions (Appendix Fig S12C-E). Such phenomena may be responsible for the reduced photosynthetic performance of those plants. Compared with NBR1-OX, *ppi1* showed even stronger reductions in photosynthetic proteins, due to the complete loss of one key TOC receptor, Toc33 (as opposed to the more modest TOC reductions seen in stressed NBR1-OX plants). This explains the big phenotypical difference between *ppi1* and NBR1-OX plants.

Discussion

Previous studies revealed that autophagy is involved in the regulation of chloroplast functions through the bulk degradation of chloroplast cargos or the turnover of whole photodamaged chloroplasts (Sun *et al*, 2021a). However, understanding of the mechanisms of chloroplast autophagy is still very preliminary, compared to autophagy in other organelles in yeast and mammals (Nakamura & Izumi, 2018; Zhuang & Jiang, 2019). In particular, little is known about the selective autophagy of chloroplast proteins due to a

lack of identified receptors and adaptors. In this study, we present multiple lines of evidence showing that NBR1 acts as a selective autophagy adaptor for the TOC complex to regulate chloroplast protein import. This regulatory mechanism is physiologically important during stress responses.

Recent studies revealed the regulation of chloroplast TOC abundance by the ubiquitin-proteasome system, which is critical for plastid biogenesis and plant stress tolerance (Ling *et al.*, 2019; Ling *et al.*, 2012). However, whether other ubiquitin-dependent pathways, such as selective autophagy, are involved in TOC regulation has remained an open question. Data presented in this study reveal that TOC component abundancies are indeed controlled by selective autophagy. Evidence for this includes the confocal microscopy detection of vacuolar TOC protein-containing puncta resembling autophagic bodies (Fig 1). Such puncta no longer existed when a key autophagy pathway component, ATG7, was missing (Fig 2A). Moreover, ATG8 was co-localized with the vacuolar TOC-containing bodies, demonstrating a functional association between TOC proteins and autophagy. Significantly, other envelope proteins such as SP1-YFP and FAX1-YFP were not localized in such TOC-containing autophagic bodies in our experimental conditions, ruling out the possibility that they were simply cargos of the well-known bulk chloroplast autophagic pathway induced upon starvation, described previously (Spitzer *et al.*, 2015; Wada *et al.*, 2009). Moreover, TOC proteins were specifically accumulated in wild-type plants treated with autophagy inhibitor, or in autophagy-deficient mutant (Fig 2B), confirming that TOC components are selective autophagy substrates.

In a screen for autophagic components in purified chloroplasts, we identified NBR1 as potential autophagy adaptor for the regulation of chloroplast cargos (Fig 3E). Although a role for plant NBR1 in selective autophagy was revealed some years ago, we have only begun to recognize its substrates in the past few years (Ji *et al.*, 2020; Thirumalaikumar *et al.*, 2021). Even less information exists concerning its substrates in chloroplasts. Subcellular fractionation analysis revealed that a large proportion of cellular ATG8 and NBR1 is associated with the chloroplast (Fig 3 and Appendix Fig S5), suggesting that chloroplast cargos are predominant targets of autophagy under the tested conditions. In particular, we detected several chloroplast envelope proteins (e.g., Toc75 and Toc33) in the list of the candidate ATG8 interactors; and interaction of NBR1 with key TOC components, Toc33, Toc159 and Toc75, was validated through co-localization, BiFC and co-IP assays (Fig 4).

Based on previous mutant analyses, NBR1 was reported to be important under specific abiotic challenges, such as heat, oxidative, salt and drought stresses (Zhou *et al.*, 2013), but its autophagic cargos under such conditions have remained largely unknown. Here, we demonstrated that *nbr1* mutant plants are more sensitive to UVB and heat stresses, whereas NBR1 overexpressors are more tolerant of such stresses (Figs 5 and 6). Given that chloroplast functions are closely linked to both of these stresses (Allorent *et al*, 2016; Dutta *et al.*, 2009), this implies that NBR1's role in chloroplasts is physiologically important. Indeed, TOC proteins are specifically regulated by NBR1 during short-term UVB and heat stresses (Figs 5 and 6); and, consistently, *nbr1* chloroplasts showed clearly enhanced import efficiency, whereas NBR1-OX chloroplasts showed compromised protein import, particularly under stress conditions, as indicated by in vitro and in vivo protein import assays (Fig 7). Furthermore, genetic experiment showed that *nbr1* mutant significantly suppressed *ppi1*, a mutant with compromised TOC import machinery (Fig 8). We interpret that other TOC components such as Toc159 accumulated at higher levels in *nbr1 ppi1* double mutant, and that this synthetically improves the double mutant phenotype relative to the *ppi1* control.

Previous work revealed that the protein import TOC machinery is regulated by the UPS in response to developmental and environmental factors (Thomson *et al*, 2020), and that the control of TOC protein levels

influences stress tolerance (Ling & Jarvis, 2015b). Our data here provide compelling evidence that selective autophagy also has a role in TOC regulation during abiotic stresses. Such regulation may be causally linked to the changes in photosynthetic protein abundance, photosynthetic performance, and chloroplast ultrastructure seen in *nbr1* mutant and NBR1 overexpressor plants (Fig 7 and Appendix Fig S12). Although plant growth may be compromised by NBR1-mediated degradation of the TOC apparatus upon short-term stress, due to reduced photosynthetic activity, such regulation may eventually ensure the survival of the plant under long-term stress conditions, possibly by suppressing excessive reactive oxygen species (ROS) (Ling & Jarvis, 2015b) (Figs 5A and 6A). Overall, our data further support the notion that the regulation of chloroplast protein import is crucial for plant stress responses and development, to meet the requirement for continuous remodelling of the organellar proteome (Demarsy *et al.*, 2014).

However, it is clear that regulation of the TOC apparatus is only one of the roles of autophagy in stress tolerance, as autophagy has been shown to influence diverse cellular compartments under stress conditions (Marshall & Vierstra, 2018). Whether NBR1 interacts with other chloroplast proteins like ATG8 (Fig 3E) remains unknown, although NBR1 is very likely to have other chloroplast targets apart from TOC proteins. Nonetheless, we do expect that ATG8 has a broader range of interactors than NBR1, as ATG8 is very likely to work with other autophagy receptors and adaptors responsible for recruiting different chloroplast cargos.

One obvious question arising from these results concerns how NBR1 is induced to recruit TOC complexes under stress conditions, as persistent degradation of TOC proteins would clearly be harmful to plants (Bauer *et al.*, 2000; Huang *et al*, 2011; Jarvis *et al.*, 1998). Recently, systematic analyses of the chloroplast ubiquitinome demonstrated broad impacts of ubiquitination on chloroplast proteins (Li *et al*, 2022; Sun *et al.*, 2022). Notably, all polyubiquitin linkage types were present in chloroplasts, and K63 was shown to be one of the most abundant types, second only to K48 (Sun *et al.*, 2022), implying that ubiquitinated chloroplast proteins can have fates other than proteasomal degradation. Ubiquitination is a key mechanism governing cellular signalling, and K63-linked polyubiquitination is particularly involved in the determination of autophagic substrate specificity in mammals and plants (Kwon & Ciechanover, 2017; Saeed *et al*, 2023). However, little is known about the role of K63 ubiquitination in plant autophagy, and it remained unclear how chloroplast protein cargos are regulated by this modification. The present study sheds light on these aspects, as it revealed that stresses like UVB exposure can cause intensive K63 ubiquitination of a key TOC component, Toc159. Interestingly, K48 ubiquitination of Toc159 was also largely enhanced by UVB, consistent with the previous finding that degradation of TOC proteins by the UPS is activated by abiotic stress (Ling & Jarvis, 2015b).

NBR1 is characterized by two domains: a ubiquitin-binding UBA domain that binds ubiquitinated proteins, and an AIM domain that links cargos to autophagic membranes (Matsumoto *et al*, 2011; Svenning *et al.*, 2011; Ustun *et al*, 2018). Intriguingly, plant NBR1 is frequently shown to target the substrates without its UBA sequences (Ji *et al.*, 2020; Thirumalaikumar *et al.*, 2021), so whether the interaction of plant NBR1 and its substrates depends on ubiquitination is still in doubt. However, we showed that deletion of the UBA domain in NBR1 indeed impaired the association between NBR1 and TOC proteins (Fig 4D). Furthermore, while expression of full length NBR1 was able to complement the heat tolerance defect in *nbr1-2, NBR1-ΔUBA* failed to do so (Appendix Fig S13). These results suggest that ubiquitin binding is also crucial for substrate recognition and physiological function of plant NBR1, similar to its mammalian homologues p62 and NBR1. p62 preferentially recognizes K63 linkages through its UBA domain (Richter *et al*, 2016). Thus, K63 modification of Toc159 may lead to its exposure to the autophagy machinery, facilitating its recognition

as a substrate. Ubiquitin linkage types are thought to be defined by specific E2/E3 combinations (Liwocha *et al*, 2021). Two E3 ligases has been uncovered to directly target chloroplast resident proteins, SP1 and PUB4 (Woodson *et al*, 2015). Although PUB4 was shown not to be responsible for autophagy (Woodson *et al.*, 2015), SP1 mediates ubiquitination of TOC components (Ling *et al.*, 2012), which may consequently promote their recognition by NBR1 and autophagic degradation. However, altering SP1 expression levels does not have obvious impacts during high light and heat stresses (Ling & Jarvis, 2015b). Therefore, it is very likely that other unknown E3 ligases may also exist to control chloroplast proteins.

Thus, our findings uncover a connection between the UPS and autophagy pathways regarding chloroplast import regulation for plant development and stress response (Appendix Fig S14). Why are TOC proteins regulated by two proteolytic pathways? One possibility is that the UPS and autophagy operate in a mutually compensatory manner to control the TOC complex. Such dual-control scenarios provide regulatory resilience and often occur in important cellular processes in mammals, such as ER stress response (Kocaturk & Gozuacik, 2018). In agreement with this idea, treatment of autophagy mutants with proteasome inhibitor resulted in even higher levels of TOC proteins (Fig 2B), indicating that the UPS and autophagy may act collaboratively to control TOC proteins. Another possibility is that the UPS and autophagy have their own priorities, depending on the severity or type of stress, as was reported in mitochondria (Scarffe *et al*, 2014). It is noteworthy that UPS activity is mainly limited to degrading individual proteins, whereas autophagy can degrade protein aggregates, multiprotein complexes, or even whole organelles (Takahashi & Arimoto, 2021). As TOC components exist in a complex, autophagy might work more efficiently by delivering quick degradation of the whole TOC complex. This might happen under some stresses, e.g., extreme light with high UVB damage, which potentially have consequences so severe or acute that they overwhelm the UPS-dependent mechanism (Ling & Jarvis, 2015b). It is even possible that the turnover of TOC complexes is a prerequisite for the selective clearance of whole organelles by autophagy (Izumi *et al.*, 2017), through a similar mechanism to that reported in mitochondria (Bertolin *et al*, 2013). However, in our stress conditions, no obvious whole-chloroplast autophagy could be observed, for example as indicated by the analysis of cpGFP transgenic lines (Appendix Fig S11). This is possibly because our UVB stress treatment was milder than conditions used previously (Izumi *et al.*, 2017), and does not cause bursts of ROS strong enough to trigger degradation of the whole damaged organelle.

In conclusion, our work has uncovered how NBR1-mediated selective autophagy plays a crucial role in the regulation of key TOC components and chloroplast protein import, which potentially contributes to plant stress tolerance. It also opens up the possibility that other chloroplast proteins may be cargos of NBR1 or other selective autophagy adaptors or receptors. This discovery reveals expanded complexity of chloroplast protein quality control systems, which are fundamental in plant physiology. These findings also suggest that the manipulation of selective chloroplast autophagy has potential applications in agriculture and in delivering carbon neutrality, through plant improvement (e.g., by enhancing environmental adaptation).

Materials and Methods

Plant materials and growth conditions

Arabidopsis thaliana Columbia-0 (Col-0) was used as the wild-type line in this study. The autophagy-deficient mutants *atg7-2* (GK655B06) and *nbr1-2* (GABI_246H08) were obtained from NASC (https://arabidopsis.info/). For the fluorescence microscopy analysis, *pToc33:YFP-Toc33* and *pToc75:YFP-Toc75* were crossed with *atg7-2* to generate the *pToc33:YFP-Toc33 atg7-2* and *pToc75:YFP-Toc75 atg7-2* lines. After stratification at 4°C for three days, plants were grown at 22°C under long day conditions (16 h light [100 µE/m^2/s] and 8 h dark cycles) on Murashige & Skoog (MS) medium supplemented with 1% sucrose and 0.8% agar in petri plates. For the induction of autophagy, 8-day-old plants were transferred onto sucrose-free MS liquid medium under dark conditions with bortezomib (5 µM), E64d (100 µM) or concanavalin A (ConA, 2 µM) and incubated for one to two additional days.

Gene identifiers

Gene sequences for the following proteins from *A. thaliana* were used experimentally in this study: NBR1 (At4g24690), Toc33 (At1g02280), Toc75 (At3g46740), Toc159 (At4g02510), OEP7 (At3g52420), ATG8 (ATG8a) (At4g21980), FAX1 (At3g57280) and Rubisco small subunit (SSU) (At1g67090).

Plasmid constructs

All primers used are listed in Table EV1. All Arabidopsis coding sequences (CDSs) were PCR-amplified from Col-0 cDNA, while CDSs of *YFP* and *mScarlet* were amplified from the p2YGW7 (Karimi *et al*, 2007) and NLS-3mScarlet vectors (Andersen *et al*, 2018), respectively. The Gateway cloning system (Invitrogen) was used for most plasmid construction, and all entry clones were verified by DNA sequencing. For protoplast transient expression analyses, *NBR1-YFP* and *FAX1-YFP* were generated using the p2GWY7 vector; *YFP-Toc33* and *YFP-Toc159* was generated using the p2YGW7 vector (Karimi *et al.*, 2007); *NBR1-CFP* was generated using the p2GWC7 vector (Karimi *et al.*, 2007); YFP tag was inserted in between Toc75 transit peptide and the N terminus of its mature part as previously reported (Chen *et al.*, 2016; Paila *et al.*, 2016) using the InFusion cloning system (Clontech), and then cloned into the P2GW7 vector (Karimi *et al.*, 2007) to generate the *YFP-Toc75* construct; haemagglutinin (HA)-tagged NBR1 (*NBR1-HA*) was generated using a modified p2GW7 vector (Karimi *et al.*, 2007) providing a C-terminal HA tag. Construct for the protoplast expression of free YFP was generated by cloning the *YFP* CDS into pBlueScript II SK− by using 5' SalI and 3' XbaI restriction sites.

To generate stable transgenic plants overexpressing NBR1 (NBR1-OX) or YFP, the corresponding CDSs without stop codon were amplified, and then cloned into the pH2GW7-based 35S-driven binary vector (Karimi *et al.*, 2007) providing a C-terminal HA tag (generating the *p35S:NBR1-HA* and *p35S:YFP-HA* constructs). Similar procedure was employed to generate the *p35S:NBR1-ΔUBA-HA* construct (residues 1-612) using the NBR1 CDS without the C terminal ubiquitin binding domains (Svenning *et al.*, 2011). To generate C-terminal mScarlet fused NBR1 (*p35S:NBR1-mScarlet*) for plant stable transformation, coding sequence of *NBR1* was amplified, and then cloned into a modified pH2GW7 vector providing a C-terminal mScarlet tag. For transgenic plants stably expressing *TOC33* or *TOC75* genes driven by their native promotors, constructs were cloned into the binary vector pCambia1301 by using 5' SalI and 3' XbaI restriction sites through the InFusion cloning system. Promotor region of *TOC33* (~2000 bp upstream region) amplified from Col-0 genomic DNA, together with the CDSs of *YFP* and *TOC33*, were used to generate *pToc33:YFP-Toc33*; and promotor region (~2000 bp upstream region) plus transit peptide region of *TOC75*

amplified from Col-0 genomic DNA, together with the CDSs of *YFP* and *TOC75* mature part, were used to generate *pToc75:YFP-Toc7*5.

The InFusion cloning system was used for most BiFC plasmid construction. CDS of *NBR1* was cloned into KpnI site of the pSAT4A-cEYFP-N1 vector (Tzfira *et al*, 2005) for *NBR1-cYFP*; CDS of *TOC33* or *TOC159* was cloned into XhoI site of the pSAT4-nEYFP-C1 vector (Tzfira *et al.*, 2005) for *nYFP-Toc33* or *nYFP-Toc159*, respectively; and CDS of OEP7 was cloned into KpnI site of the pSAT4A-nEYFP-N1 vector (Tzfira *et al.*, 2005) for *OEP7-nYFP*. The nYFP tag was inserted in between Toc75 transit peptide and the N terminus of its mature part using a similar procedure as described above for making *YFP-Toc75*, to generate the *nYFP-Toc75* construct through the p2GW7 vector using the Gateway cloning system.

Transient assays and stable plant transformation

Protoplast isolation and transient assays were carried out as described previously (Ling *et al.*, 2019; Wu *et al*, 2009). For YFP fluorescence and immunoprecipitation assays, 0.1 mL (10^5) or 1 mL (10^6) of protoplast were transfected with 5 µg or 100 µg of DNA, respectively; the fluorescence signals were analyzed after 15-18 h. When required, Bortezomib (Selleckchem) or ConA (APExBIO) was added to the protoplast culture medium to a final concentration of 5 µM or 1 µM, respectively.

The transgenic plants were generated by Agrobacterium-mediated transformation (Huang *et al.*, 2011). Transformants were selected using MS medium containing 50 µg/mL hygromycin B (for the pCambia1301- or pH2GW7-based constructs). Approximately ten independent T2 lines were analyzed per construct, and one representative line with a single T-DNA insertion (which showed a 3:1 segregation on selective MS medium in the T2 generation) were chosen for further analysis.

UVB treatment

To examine UVB stress tolerance in Arabidopsis, plants were grown in soil under normal growth condition for eight days, and then treated with white light (18 µE/m^2/s) plus broadband UVB (5 µE/m^2/s) as previous described (Liang *et al*, 2020) for 3 h. The treated plants were then allowed to recover for 7 days under normal growth condition prior to phenotypical analysis. Alternatively, treated plants were recovered for up to one day for immunoblotting analysis, to avoid strong growth defect which may lead to secondary effect. For the analyses of photosynthetic performance (F_v/F_m), chloroplast ultrastructure (TEM) and in vivo protein import (FRAP), eight-day-old plants grown in petri plates were treated with broadband UVB for 4 h, and recovered for one day before further analyses.

Heat treatment

To examine heat tolerance stress in Arabidopsis, plants were grown in soil under normal growth condition for four weeks, then incubated at 42°C for 17 h, and finally recovered under normal growth condition for two days before phenotypical analysis. For short-term heat stress analysis, eight-day-old plants grown in petri plates were incubated at 42°C for 4 h, and then recovered for up to one day before immunoblotting analysis.

Measurement of photosynthetic performance

The UVB treated plants grown on agar plates were recovered for up to one day, and leaves were dark adapted for a minimum of 30 min before the photochemical activity was examined in individual leaves. Maximum photochemical efficiency of photosystem II (F_v/F_m) was determined by measuring chlorophyll

fluorescence with a fluorescence imaging system (Closed FluorCam FC 800-C/1010 GFP, Photon Systems Instruments, Czech Republic) as described previously (Liu *et al*, 2020). Three experiments were performed, and approximately ten seedlings were analyzed per genotype in each experiment.

Chlorophyll measurements

To measure chlorophyll content, UVB-treated plants grown in soil were recovered for up to one day, then harvested, weighted, frozen in liquid nitrogen, and ground to powder using a motor with precooled pestle. Chlorophylls were extracted from ~10 mg frozen tissue powder in 1 mL 80% acetone through vigorous vortexing, followed by incubation at 4°C for 30 min with slow rotation. The extract was centrifuged at 1,000 × *g* for 10 min, and the supernatant was used for chlorophyll determination. Chlorophyll concentrations were measured using a spectrophotometer as described previously (Lichtenthaler, 1987).

Microscopy

Fluorescence images were captured using TCS SP8 (Leica Ltd.) or SpinSR (Olympus Ltd.) laser-scanning confocal microscope, as described previously (Hu *et al*, 2022; Liu *et al*, 2022). All experiments were conducted at least twice with the same results, and typical images are presented. All images were captured using the same settings to enable comparisons. For the observation of autophagosomes, Arabidopsis protoplasts expressing the YFP-tagged TOC proteins were analyzed by confocal microscopy following ConA treatment for 4 h. Alternatively, eight-day-old transgenic Arabidopsis seedlings stably expressing YFP-tagged TOC proteins were treated with ConA for 2 d, and then analyzed by confocal microscopy.

Transmission electron microscopy was performed as described previously (Huang *et al.*, 2011). Measurements were taken using at least 30 different chloroplasts per genotype and are representative of three individuals per genotype. Chloroplast shape was determined as described (Huang *et al.*, 2011) based on the length/width ratio. Numbers of thylakoid lamellae per granal stack were counted as previously described (Huang *et al.*, 2011; Ling *et al.*, 2012). Numbers of starch granules were estimated as described (Crumpton-Taylor *et al*, 2012).

Chloroplast isolation and in vitro protein import assay

Chloroplasts were isolated from 12-day-old in vitro grown plants (or, when stated, from protoplasts). Isolations and protein import were performed as described previously (Aronsson & Jarvis, 2002; Fitzpatrick & Keegstra, 2001; Huang *et al.*, 2011). The presented import data are representative for four independent experiments.

SDS-PAGE, immunoblotting and immunoprecipitation

Sodium dodecyl sulphate-polyacrylamide gel electrophoresis (SDS-PAGE) and immunoblotting were performed essentially as described before (Kovacheva *et al.*, 2005). Primary antibodies were as follows. To detect TOC or TIC proteins, we employed: anti-atToc75-III POTRA-domain antibody (Huang *et al.*, 2011); anti-atToc159 A-domain antibody (Bauer *et al.*, 2000); anti-atToc33 pepitide antibody (Aronsson *et al*, 2003); anti-atTic110 stromal antibody (Inaba *et al*, 2005); anti-atTic40 stromal antibody (Kasmati *et al*, 2011). To detect proteins of other cellular compartments, we employed: ATG8 (cytosol; AS14 2769, Agrisera); NBR1 (cytosol; AS142805, Agrisera); PEPC (cytosol; AS09458, Agrisera) anti-Actin (cytosol; LF208, Epizyme); anti-PsaD (PSI subunit; PAB01004, Orizymes); anti-PsbP (PSII subunit; PA02014, Orizymes); and anti-AtpA (chloroplast thylakoid; PAB04001, Orizymes). Other primary antibodies employed were: K48-linkage Specific Polyubiquitin antibody (8081S, CST); K63-linkage Specific Polyubiquitin antibody (5621S, CST); anti-

HA tag antibody (sigma, H6908); anti-GFP antibody (detects both GFP and YFP; Sigma, SAB4301138). We used Tic110 or Actin as loading controls.

Secondary antibodies were polyclonal goat anti-rabbit IgG conjugated with horseradish peroxidase (Santa Cruz Biotechnology). Chemiluminescence was detected using ECL Plus Western Blotting Detection Reagents (GE Healthcare) and a Tanon 5200 imager (Tanon). Band intensities were quantified using ImageJ. Quantification data were from at least three experiments which showing a similar trend. Typical images are shown in all figures.

For the immunoprecipitation of NBR1-HA and NBR1-ΔUBA-HA, *p35S:NBR1-HA* and *p35S:NBR1*-ΔUBA-*HA* transgenic plants were used for subsequent analysis. To stimulate the recruitment of TOC components by NBR1, eight-day-old transgenic seedlings were exposed to UVB for four hours before protein extraction. Total protein (~100 mg) was then extracted from these seedlings in IP buffer (25 mM Tris-HCl, pH 7.5, 150 mM NaCl, 1 mM EDTA, 10% glycerol, 1% Triton X-100) containing 0.5% PIC (Sigma) and 5 μM bortezomib, and then centrifuged at 10,000 × *g* for 10 min at 4°C. The clear lysate was then incubated with 50 μL anti-HA beads (Thermofisher) at 4°C for 4-6 h with slow rotation. After three washes with 500 μL washing buffer (25 mM Tris-HCl, pH 7.5, 150 mM NaCl, 1 mM EDTA, 10% glycerol, 0.5% Triton X-100), bound proteins were eluted by boiling in 2× SDS-PAGE loading buffer (50 mM Tris-HCl, pH 6.8, 20% glycerol, 1% SDS, 0.1 M DTT) for 5 min, and analyzed by SDS-PAGE and immunoblotting. Transgenic plants of *p35S:YFP-HA* were set as a negative control. A similar procedure was adopted for the immunoprecipitation of YFP-tagged proteins, except that 50 μL anti-GFP magnetic beads (ChromoTek) was used to precipitate YFP tagged proteins from isolated chloroplasts.

Ubiquitination of Toc159 in vivo was assessed as described previously (Ling *et al.*, 2012), except that the protein was extracted from eight-day-old WT plants grown in petri plates treated with or without UVB for four hours, and that anti-atToc159 was used to precipitate endogenous Toc159 protein (or its preimmune serum as a negative control). Ubiquitinated Toc159 was detected by anti-K48-ubiquitin and anti-K63-ubiquitin antibodies.

Mass spectrometry analysis and function annotation

For the IP of YFP-ATG8, 1.5 mL protoplasts were used for the transient expression of YFP-ATG8 or free YFP as a negative control. Transfected protoplasts were let sit in the dark for 15 h followed by incubation with 5 μM bortezomib and 1 μM ConA for another 4 h. Protoplasts were equilibrated with HEPES-sorbitol buffer (50 mM HEPES-KOH pH 7.3, 330 mM sorbitol), and chloroplasts were isolated from the protoplasts as described previously (Fitzpatrick & Keegstra, 2001). IP was conducted as described above, and the eluted protein samples were analyzed by LC-MS/MS, which was performed by Shanghai Luming Biotechnology Co., Ltd.

Immunoprecipitated proteins were denatured and alkylated with 30 μL urea buffer (8 M urea, 50 mM ammonium bicarbonate [AB], 10 mM DTT, 0.2% protease inhibitor [Sigma, P8340]), and incubated at 55°C for 30 min, followed by adding 15 mM iodoacetamide aqueous solution for another 30 min in the dark at room temperature. The digestion solution was diluted to <1 M urea upon addition of trypsin (Promega, V511A; 200 ng in 300 μL of 1 M urea, 25 mM AB, 1 mM $CaCl_2$), prior to incubation at 37°C overnight. After digestion, the eluate fractions were collected by centrifugation at 14,000 × *g* for 5 min at 25°C.

Resulting tryptic peptides were analyzed on an EASY-nano-LC 1200 system (Thermo Fisher) connected to a Q Exactive mass spectrometer (Thermo Fisher) through an EASY-Spray nano-electrospray ion source

(Thermo Fisher). The peptides were initially trapped on an RP-C18 Trap column (100 µm i.d. x 20 mm, Thermo Fisher) using solvent A (0.1% formic acid in water). Trapped peptides were separated on an RP-C18 Analysis column (75 µm i.d. × 150 mm, Thermo Fisher) using a linear gradient (length: 60 minutes, 18% to 30% solvent B [0.1% formic acid, 5% DMSO in acetonitrile], flow rate: 300 nL/min). The separated peptides were electrosprayed directly into the mass spectrometer operating in a data-dependent mode. Full scan MS spectra were acquired in the Orbitrap (scan range 300-1600 m/z, resolution 35000, AGC target 3e6, maximum injection time 50 ms). After the MS scans, the ten most intense peaks were selected for HCD fragmentation at 28% of normalized collision energy. HCD spectra were also acquired in the Orbitrap (resolution 17500, AGC target 5e4, maximum injection time 50 ms).

The MS raw data for each sample were combined and searched using ProteomeDiscover (v2.4, Thermo Fisher) software against an Arabidopsis UniProt database (UniProt, 2021). Trypsin was chosen as the enzyme with a maximum of two missed cleavages allowed. Precursor and fragment mass error tolerances were set at 20 ppm and 0.1 Da, respectively. All matched MS/MS spectra were filtered by mass accuracy and matching scores to reduce protein FDR to ≤1%, based on the target-decoy strategy using a reversed database. Relative protein quantification was performed through label-free quantification analysis and the search engine was Andromeda. Quantitation was carried out only for proteins with two or more unique peptide matches.

Proteins identified by LC-MS/MS were manually annotated with respect to subcellular localization, and function. Information on protein subcellular localization was searched for sequentially and manually in several public databases (TAIR (Lamesch *et al*, 2012), UniProt (UniProt, 2021), NCBI (Coordinators, 2018), PPDB (Sun *et al*, 2009)) and in the appropriate literature, in order to annotate well-characterized chloroplast proteins. Alternatively, TargetP (Almagro Armenteros *et al*, 2019) prediction tools were used to test for the presence of a transit peptide (a typical feature of chloroplast proteins); or the SUBA4 database (Hooper *et al*, 2017) was used, which provides information on subcellular localization from published proteomic or fluorescent protein fusion datasets.

FRAP assay

FRAP of Arabidopsis hypocotyl chloroplasts was performed on a Leica TCS SP8 microscope using a 60X/NA1.2 water objective. Chloroplasts were bleached using a laser intensity of 20% at 488 nm with 3 repeats. Images were acquired using LAX software (Leica). Fluorescence recovery was recorded continuously for 300 s (3 s interval with 100 repeats) after bleaching. Analyses of the fluorescence intensity of bleached region, reference region and background region were carried out using cellSens imaging software (Olympus), and recovery curves were drawn using the cellSens FRAP plugin. The graph shown were finally drawn with GraphPad Prism software.

Statistical analysis

Statistical calculations (mean, standard error of the mean, *t*-test) were performed using GraphPad Prism software. Statistical significance of differences between two experimental groups was assessed by using an unpaired two-tailed Student's *t*-test. Differences between two datasets were considered significant at $P < 0.05$.

Data availability:

All data needed to evaluate the conclusions in the paper are present in the paper and/or the Appendix. The mass spectrometry proteomics data have been deposited to the Integrated Proteome Resources (iProX, https://www.iprox.cn/) with the identifier PXD040844.

Acknowledgements:

We thank X. Gao, Z. Zhang, J. Li and L. Xu (Center for Excellence in Molecular Plant Sciences [CEMPS] EM Laboratory) for electron microscopy; H. Liu and C. Shi (CEMPS) for the technical assistance with UVB treatment and photosynthetic measurement; Z. Yao for the assistance of mass spectrometry data analysis; M. Izumi (RIKEN, Japan) for the *p35S:cpGFP* seeds; F. Kessler (University of Neuchâtel) for the Toc159 antibody; F. Zhou (CEMPS) for the NLS-3mScarlet vector; and SIGnAL and NASC for the *atg7-2* and *nbr1-2* alleles. This work was supported by grants from the Chinese Academy of Sciences (CAS), CEMPS/Institute of Plant Physiology and Ecology to Q.L.; CAS National Key Laboratory of Plant Molecular Genetics to Q.L.; CAS Strategic Priority Research Program (Type-B; project XDB27020107) to Q.L.; the National Natural Science Foundation of China (NSFC) (project 32070260) to Q.L.; NSFC (project 32100193) to H.Z.; UK Research and Innovation Biotechnology and Biological Sciences Research Council (UKRI-BBSRC; PhD studentship BB/M015165/1 and project grants BB/N006372/1, BB/R009333/1, BB/R016984/1 and BB/V007300/1) to R.P.J..

Disclosure and competing interests statement

The authors declare that they have no conflict of interest.

References:

Agne B, Andres C, Montandon C, Christ B, Ertan A, Jung F, Infanger S, Bischof S, Baginsky S, Kessler F (2010) The acidic A-domain of Arabidopsis Toc159 occurs as a hyperphosphorylated protein. *Plant Physiol* 153: 1016-1030

Allorent G, Lefebvre-Legendre L, Chappuis R, Kuntz M, Truong TB, Niyogi KK, Ulm R, Goldschmidt-Clermont M (2016) UV-B photoreceptor-mediated protection of the photosynthetic machinery in Chlamydomonas reinhardtii. *ProcNatl Acad Sci USA* 113: 14864-14869

Almagro Armenteros JJ, Salvatore M, Emanuelsson O, Winther O, von Heijne G, Elofsson A, Nielsen H (2019) Detecting sequence signals in targeting peptides using deep learning. *Life Sci Alliance* 2: e201900429

Andersen TG, Naseer S, Ursache R, Wybouw B, Smet W, De Rybel B, Vermeer JEM, Geldner N (2018) Diffusible repression of cytokinin signalling produces endodermal symmetry and passage cells. *Nature* 555: 529-533

Aronsson H, Combe J, Jarvis P (2003) Unusual nucleotide-binding properties of the chloroplast protein import receptor, atToc33. *FEBS Lett* 544: 79-85

Aronsson H, Jarvis P (2002) A simple method for isolating import-competent *Arabidopsis* chloroplasts. *FEBS Lett* 529: 215-220

Avila-Ospina L, Moison M, Yoshimoto K, Masclaux-Daubresse C (2014) Autophagy, plant senescence, and nutrient recycling. *J Exp Bot* 65: 3799-3811

Avin-Wittenberg T, Michaeli S, Honig A, Galili G (2012) ATI1, a newly identified atg8-interacting protein, binds two different Atg8 homologs. *Plant Signal Behav* 7: 685-687

Bauer J, Chen K, Hiltbrunner A, Wehrli E, Eugster M, Schnell D, Kessler F (2000) The major protein import receptor of plastids is essential for chloroplast biogenesis. *Nature* 403: 203-207

Bédard J, Kubis S, Bimanadham S, Jarvis P (2007) Functional similarity between the chloroplast translocon component, Tic40, and the human co-chaperone, Hsp70-interacting protein (Hip). *J Biol Chem* 282: 21404-21414

Bertolin G, Ferrando-Miguel R, Jacoupy M, Traver S, Grenier K, Greene AW, Dauphin A, Waharte F, Bayot A, Salamero J *et al* (2013) The TOMM machinery is a molecular switch in PINK1 and PARK2/PARKIN-dependent mitochondrial clearance. *Autophagy* 9: 1801-1817

Chen H, Dong J, Wang T (2021) Autophagy in plant abiotic stress management. *Int J Mol Sci* 22

Chen YL, Chen LJ, Li HM (2016) Polypeptide transport domains of the Toc75 channel protein are located in the intermembrane space of chloroplasts. *Plant Physiol* 172: 235-243

Coordinators NR (2018) Database resources of the National Center for Biotechnology Information. *Nucleic Acids Res* 46: D8-D13

Craggs TD (2009) Green fluorescent protein: structure, folding and chromophore maturation. *Chem Soc Rev* 38: 2865-2875

Crumpton-Taylor M, Grandison S, Png KM, Bushby AJ, Smith AM (2012) Control of starch granule numbers in Arabidopsis chloroplasts. *Plant Physiol* 158: 905-916

Demarsy E, Lakshmanan AM, Kessler F (2014) Border control: selectivity of chloroplast protein import and regulation at the TOC-complex. *Front Plant Sci* 5: 483

Dikic I, Elazar Z (2018) Mechanism and medical implications of mammalian autophagy. *Nat Rev Mol Cell Biol* 19: 349-364

Dutta S, Mohanty S, Tripathy BC (2009) Role of temperature stress on chloroplast biogenesis and protein import in pea. *Plant Physiol* 150: 1050-1061

Fitzpatrick LM, Keegstra K (2001) A method for isolating a high yield of *Arabidopsis* chloroplasts capable of efficient import of precursor proteins. *Plant J* 27: 59-65

Grimmer J, Helm S, Dobritzsch D, Hause G, Shema G, Zahedi RP, Baginsky S (2020) Mild proteasomal stress improves photosynthetic performance in Arabidopsis chloroplasts. *Nat Commun* 11: 1662

803 Hooper CM, Castleden IR, Tanz SK, Aryamanesh N, Millar AH (2017) SUBA4: the interactive data analysis centre
804 for Arabidopsis subcellular protein locations. *Nucleic Acids Res* 45: D1064-D1074
805 Hu Y, Ding Y, Cai B, Qin X, Wu J, Yuan M, Wan S, Zhao Y, Xin XF (2022) Bacterial effectors manipulate plant abscisic
806 acid signaling for creation of an aqueous apoplast. *Cell Host Microbe* 30: 518-529 e516
807 Huang W, Ling Q, Bédard J, Lilley K, Jarvis P (2011) In vivo analyses of the roles of essential Omp85-related
808 proteins in the chloroplast outer envelope membrane. *Plant Physiol* 157: 147-159
809 Inaba T, Alvarez-Huerta M, Li M, Bauer J, Ewers C, Kessler F, Schnell DJ (2005) Arabidopsis Tic110 is essential for
810 the assembly and function of the protein import machinery of plastids. *Plant Cell* 17: 1482-1496
811 Ishida H, Yoshimoto K, Izumi M, Reisen D, Yano Y, Makino A, Ohsumi Y, Hanson MR, Mae T (2008) Mobilization of
812 rubisco and stroma-localized fluorescent proteins of chloroplasts to the vacuole by an ATG gene-dependent
813 autophagic process. *Plant Physiol* 148: 142-155
814 Izumi M, Ishida H, Nakamura S, Hidema J (2017) Entire photodamaged chloroplasts are transported to the central
815 vacuole by autophagy. *Plant Cell* 29: 377-394
816 Jarvis P, Chen LJ, Li H, Peto CA, Fankhauser C, Chory J (1998) An *Arabidopsis* mutant defective in the plastid
817 general protein import apparatus. *Science* 282: 100-103
818 Jarvis P, López-Juez E (2013) Biogenesis and homeostasis of chloroplasts and other plastids. *Nat Rev Mol Cell Biol*
819 14: 787-802
820 Ji C, Zhou J, Guo R, Lin Y, Kung CH, Hu S, Ng WY, Zhuang X, Jiang L (2020) AtNBR1 is a selective autophagic receptor
821 for AtExo70E2 in arabidopsis. *Plant Physiol* 184: 777-791
822 Karimi M, Depicker A, Hilson P (2007) Recombinational cloning with plant gateway vectors. *Plant Physiol* 145:
823 1144-1154
824 Kasmati AR, Töpel M, Patel R, Murtaza G, Jarvis P (2011) Molecular and genetic analyses of Tic20 homologues in
825 *Arabidopsis thaliana* chloroplasts. *Plant J* 66: 877-889
826 Kirkin V, Rogov VV (2019) A diversity of selective autophagy receptors determines the specificity of the autophagy
827 pathway. *Mol Cell* 76: 268-285
828 Kocaturk NM, Gozuacik D (2018) Crosstalk between mammalian autophagy and the ubiquitin-proteasome
829 system. *Front Cell Dev Biol* 6: 128
830 Kovacheva S, Bédard J, Patel R, Dudley P, Twell D, Ríos G, Koncz C, Jarvis P (2005) *In vivo* studies on the roles of
831 Tic110, Tic40 and Hsp93 during chloroplast protein import. *Plant J* 41: 412-428
832 Kwon YT, Ciechanover A (2017) The Ubiquitin Code in the Ubiquitin-Proteasome System and Autophagy. *Trends*
833 *in Biochemical Sciences* 42: 873-886
834 Lamesch P, Berardini TZ, Li D, Swarbreck D, Wilks C, Sasidharan R, Muller R, Dreher K, Alexander DL, Garcia-
835 Hernandez M *et al* (2012) The Arabidopsis Information Resource (TAIR): improved gene annotation and new tools.
836 *Nucleic Acids Res* 40: D1202-1210
837 Lee S, Lee DW, Lee Y, Mayer U, Stierhof YD, Jurgens G, Hwang I (2009) Heat shock protein cognate 70-4 and an
838 E3 ubiquitin ligase, CHIP, mediate plastid-destined precursor degradation through the ubiquitin-26S proteasome
839 system in *Arabidopsis*. *Plant Cell* 21: 3984-4001
840 Li HM, Teng YS (2013) Transit peptide design and plastid import regulation. *Trends Plant Sci* 18: 360-366
841 Li J, Yuan J, Li Y, Sun H, Ma T, Huai J, Yang W, Zhang W, Lin R (2022) The CDC48 complex mediates ubiquitin-
842 dependent degradation of intra-chloroplast proteins in plants. *Cell Rep* 39: 110664
843 Liang T, Shi C, Peng Y, Tan H, Xin P, Yang Y, Wang F, Li X, Chu J, Huang J *et al* (2020) Brassinosteroid-activated BRI1-
844 EMS-SUPPRESSOR 1 inhibits flavonoid biosynthesis and coordinates growth and UV-B stress responses in plants.
845 *Plant Cell* 32: 3224-3239
846 Lichtenthaler HK (1987) Chlorophylls and carotenoids: Pigments of photosynthetic biomembranes. In: *Methods*

in Enzymology, pp. 350-382. Academic Press:
Ling Q, Broad W, Trosch R, Topel M, Demiral Sert T, Lymperopoulos P, Baldwin A, Jarvis RP (2019) Ubiquitin-dependent chloroplast-associated protein degradation in plants. *Science* 363
Ling Q, Huang W, Baldwin A, Jarvis P (2012) Chloroplast biogenesis is regulated by direct action of the ubiquitin-proteasome system. *Science* 338: 655-659
Ling Q, Jarvis P (2015a) Functions of plastid protein import and the ubiquitin-proteasome system in plastid development. *Biochim Biophys Acta* 1847: 939-948
Ling Q, Jarvis P (2015b) Regulation of chloroplast protein import by the ubiquitin E3 ligase SP1 is important for stress tolerance in plants. *Curr Biol* 25: 2527-2534
Ling Q, Sadali NM, Soufi Z, Zhou Y, Huang B, Zeng Y, Rodriguez-Concepcion M, Jarvis RP (2021) The chloroplast-associated protein degradation pathway controls chromoplast development and fruit ripening in tomato. *Nat Plants* 7: 655-666
Liu PC, Peacock WJ, Wang L, Furbank R, Larkum A, Dennis ES (2020) Leaf growth in early development is key to biomass heterosis in Arabidopsis. *J Exp Bot* 71: 2439-2450
Liu Z, Osterlund I, Ruhnow F, Cao Y, Huang G, Cai W, Zhang J, Liang W, Nikoloski Z, Persson S *et al* (2022) Fluorescent cytoskeletal markers reveal associations between the actin and microtubule cytoskeleton in rice cells. *Development*: 200415
Liwocha J, Krist DT, van der Heden van Noort GJ, Hansen FM, Truong VH, Karayel O, Purser N, Houston D, Burton N, Bostock MJ *et al* (2021) Linkage-specific ubiquitin chain formation depends on a lysine hydrocarbon ruler. *Nat Chem Biol* 17: 272-279
Marshall RS, Vierstra RD (2018) Autophagy: The Master of Bulk and Selective Recycling. *Annu Rev Plant Biol* 69: 173-208
Matsumoto G, Wada K, Okuno M, Kurosawa M, Nukina N (2011) Serine 403 phosphorylation of p62/SQSTM1 regulates selective autophagic clearance of ubiquitinated proteins. *Mol Cell* 44: 279-289
Michaeli S, Honig A, Levanony H, Peled-Zehavi H, Galili G (2014) Arabidopsis ATG8-INTERACTING PROTEIN1 is involved in autophagy-dependent vesicular trafficking of plastid proteins to the vacuole. *Plant Cell* 26: 4084-4101
Nakamura S, Hagihara S, Otomo K, Ishida H, Hidema J, Nemoto T, Izumi M (2021) Autophagy contributes to the quality control of leaf mitochondria. *Plant Cell Physiol* 62: 229-247
Nakamura S, Hidema J, Sakamoto W, Ishida H, Izumi M (2018) Selective Elimination of Membrane-Damaged Chloroplasts via Microautophagy. *Plant Physiol* 177: 1007-1026
Nakamura S, Izumi M (2018) Regulation of chlorophagy during photoinhibition and senescence: Lessons from mitophagy. *Plant Cell Physiol* 59: 1135-1143
Nakatogawa H (2020) Mechanisms governing autophagosome biogenesis. *Nat Rev Mol Cell Biol* 21: 439-458
Nolan TM, Brennan B, Yang M, Chen J, Zhang M, Li Z, Wang X, Bassham DC, Walley J, Yin Y (2017) Selective autophagy of BES1 mediated by DSK2 balances plant growth and survival. *Dev Cell* 41: 33-46 e37
Otegui MS (2018) Vacuolar degradation of chloroplast components: autophagy and beyond. *J Exp Bot* 69: 741-750
Paila YD, Richardson LG, Inoue H, Parks ES, McMahon J, Inoue K, Schnell DJ (2016) Multi-functional roles for the polypeptide transport associated domains of Toc75 in chloroplast protein import. *eLife* 5: e12631
Palikaras K, Lionaki E, Tavernarakis N (2018) Mechanisms of mitophagy in cellular homeostasis, physiology and pathology. *Nat Cell Biol* 20: 1013-1022
Richardson LGL, Singhal R, Schnell DJ (2017) The integration of chloroplast protein targeting with plant developmental and stress responses. *BMC Biol* 15: 118
Richter B, Sliter DA, Herhaus L, Stolz A, Wang C, Beli P, Zaffagnini G, Wild P, Martens S, Wagner SA *et al* (2016)

Phosphorylation of OPTN by TBK1 enhances its binding to Ub chains and promotes selective autophagy of damaged mitochondria. *Proc Natl Acad Sci USA* 113: 4039-4044

Rochaix JD (2022) Chloroplast protein import machinery and quality control. *FEBS J*

Rolland N, Curien G, Finazzi G, Kuntz M, Marechal E, Matringe M, Ravanel S, Seigneurin-Berny D (2012) The biosynthetic capacities of the plastids and integration between cytoplasmic and chloroplast processes. *Annu Rev Genet* 46: 233-264

Saeed B, Deligne F, Brillada C, Dunser K, Ditengou FA, Turek I, Allahham A, Grujic N, Dagdas Y, Ott T *et al* (2023) K63-linked ubiquitin chains are a global signal for endocytosis and contribute to selective autophagy in plants. *Current Biology* 33: 1-9

Scarffe LA, Stevens DA, Dawson VL, Dawson TM (2014) Parkin and PINK1: much more than mitophagy. *Trends Neurosci* 37: 315-324

Schwenkert S, Fernie AR, Geigenberger P, Leister D, Mohlmann T, Naranjo B, Neuhaus HE (2022) Chloroplasts are key players to cope with light and temperature stress. *Trends Plant Sci* 27: 577-587

Shanmugabalaji V, Chahtane H, Accossato S, Rahire M, Gouzerh G, Lopez-Molina L, Kessler F (2018) Chloroplast biogenesis controlled by DELLA-TOC159 interaction in early plant development. *Curr Biol* 28: 2616-2623 e2615

Shi C, Liu H (2021) How plants protect themselves from ultraviolet-B radiation stress. *Plant Physiol* 187: 1096-1103

Shi LX, Theg SM (2013) The chloroplast protein import system: from algae to trees. *Biochim Biophys Acta* 1833: 314-331

Shin KD, Lee HN, Chung T (2014) A revised assay for monitoring autophagic flux in Arabidopsis thaliana reveals involvement of AUTOPHAGY-RELATED9 in autophagy. *Mol Cells* 37: 399-405

Spitzer C, Li F, Buono R, Roschzttardtz H, Chung T, Zhang M, Osteryoung KW, Vierstra RD, Otegui MS (2015) The endosomal protein CHARGED MULTIVESICULAR BODY PROTEIN1 regulates the autophagic turnover of plastids in Arabidopsis. *Plant Cell* 27: 391-402

Stephani M, Dagdas Y (2020) Plant selective autophagy-still an uncharted territory with a lot of hidden gems. *J Mol Biol* 432: 63-79

Sun JL, Li JY, Wang MJ, Song ZT, Liu JX (2021a) Protein quality control in plant organelles: Current progress and future perspectives. *Mol Plant* 14: 95-114

Sun Q, Zybailov B, Majeran W, Friso G, Olinares PD, van Wijk KJ (2009) PPDB, the plant proteomics database at cornell. *Nucleic Acids Res* 37: D969-D974

Sun S, Feng L, Chung KP, Lee KM, Cheung HH, Luo M, Ren K, Law KC, Jiang L, Wong KB *et al* (2021b) Mechanistic insights into an atypical interaction between ATG8 and SH3P2 in Arabidopsis thaliana. *Autophagy* 17: 1-17

Sun Y, Yao Z, Ye Y, Fang J, Chen H, Lyu Y, Broad W, Fournier M, Chen G, Hu Y *et al* (2022) Ubiquitin-based pathway acts inside chloroplasts to regulate photosynthesis. *Sci Adv* 8: eabq7352

Svenning S, Lamark T, Krause K, Johansen T (2011) Plant NBR1 is a selective autophagy substrate and a functional hybrid of the mammalian autophagic adapters NBR1 and p62/SQSTM1. *Autophagy* 7: 993-1010

Takahashi D, Arimoto H (2021) Selective autophagy as the basis of autophagy-based degraders. *Cell Chem Biol* 28: 1061-1071

Thirumalaikumar VP, Gorka M, Schulz K, Masclaux-Daubresse C, Sampathkumar A, Skirycz A, Vierstra RD, Balazadeh S (2021) Selective autophagy regulates heat stress memory in Arabidopsis by NBR1-mediated targeting of HSP90.1 and ROF1. *Autophagy* 17: 2184-2199

Thomson SM, Pulido P, Jarvis RP (2020) Protein import into chloroplasts and its regulation by the ubiquitin-proteasome system. *Biochem Soc Trans* 48: 71-82

Tzfira T, Tian GW, Lacroix B, Vyas S, Li J, Leitner-Dagan Y, Krichevsky A, Taylor T, Vainstein A, Citovsky V (2005) pSAT

vectors: a modular series of plasmids for autofluorescent protein tagging and expression of multiple genes in plants. *Plant Mol Biol* 57: 503-516

UniProt C (2021) UniProt: the universal protein knowledgebase in 2021. *Nucleic Acids Res* 49: D480-D489

Ustun S, Hafren A, Liu Q, Marshall RS, Minina EA, Bozhkov PV, Vierstra RD, Hofius D (2018) Bacteria exploit autophagy for proteasome degradation and enhanced virulence in plants. *Plant Cell* 30: 668-685

Vierstra RD (2009) The ubiquitin-26S proteasome system at the nexus of plant biology. *Nat Rev Mol Cell Biol* 10: 385-397

Wada S, Ishida H, Izumi M, Yoshimoto K, Ohsumi Y, Mae T, Makino A (2009) Autophagy plays a role in chloroplast degradation during senescence in individually darkened leaves. *Plant Physiol* 149: 885-893

Wan C, Ling Q (2022) Functions of autophagy in chloroplast protein degradation and homeostasis. *Frontiers in plant science* 13: 993215

Woodson JD, Joens MS, Sinson AB, Gilkerson J, Salome PA, Weigel D, Fitzpatrick JA, Chory J (2015) Ubiquitin facilitates a quality-control pathway that removes damaged chloroplasts. *Science* 350: 450-454

Wu FH, Shen SC, Lee LY, Lee SH, Chan MT, Lin CS (2009) Tape-Arabidopsis Sandwich - a simpler Arabidopsis protoplast isolation method. *Plant Methods* 5: 16

Zhou J, Wang J, Cheng Y, Chi YJ, Fan B, Yu JQ, Chen Z (2013) NBR1-mediated selective autophagy targets insoluble ubiquitinated protein aggregates in plant stress responses. *PLoS Genet* 9: e1003196

Zhuang X, Jiang L (2019) Chloroplast degradation: Multiple routes into the vacuole. *Front Plant Sci* 10: 359

Main Figure Legends

Figure 1. Components of the TOC complex are selectively processed by autophagy.

A, C Presence of TOC proteins in the central vacuole of protoplasts. Arabidopsis protoplasts expressing the YFP-tagged chloroplast proteins were analyzed by confocal microscopy following ConA treatment for four hours. Representative images are shown (A). Chlorophyll autofluorescence was used to determine the localization of the YFP fluorescence signals relative to the chloroplasts. Signals for SP1-YFP and FAX1-YFP, which here are control proteins, were only present at the chloroplast envelope. Accumulation of YFP puncta in the central vacuole is indicated by the arrowheads. Scale bar, 10 µm. In addition, the numbers of YFP puncta in the central vacuole per protoplast were quantified (B). All values are means ± SEM from three experiments.

C ATG8 and TOC proteins colocalized in the central vacuole of protoplasts. Arabidopsis protoplasts coexpressing the CFP-ATG8 and YFP-tagged proteins were analyzed by confocal microscopy following ConA treatment for four hours. Representative images are shown. Accumulation of punctate bodies of overlapping fluorescence is indicated by the arrowheads. Scale bars: 10 µm.

D Presence of TOC proteins in the central vacuole of Arabidopsis leaf and hypocotyl cells. Eight-day-old transgenic Arabidopsis seedlings stably expressing *pToc33:YFP-Toc33* or *pToc75:YFP-Toc75* were treated with ConA for two days, and then analyzed by confocal microscopy. Accumulation of YFP puncta in the central vacuole is indicated by the arrowheads. Scale bar, 10 µm.

Figure 2. Degradation of TOC complex is affected upon autophagy inhibition.

A Lack of TOC proteins in the central vacuole of *atg7-2* mutant hypocotyl cells. Eight-day-old transgenic Arabidopsis seedlings stably expressing *pToc33:YFP-Toc33* and *pToc75:YFP-Toc75* in the *atg7-2* mutant background were treated with ConA for two days, and then analyzed by confocal microscopy. Note that YFP-Toc33 and YFP-Toc75 bodies (arrowheads) were retained at plastid bridges and extensions, and not released into the vacuole, as occurs in the WT background (see Fig 1D, which acts as a positive control for this experiment). Scale bar, 10 µm.

B, C Autophagy inhibition affected accumulation of TOC proteins. Eight-day-old wild-type (WT) and *atg7-2* plants were treated respectively with proteasome inhibitor, bortezomib (Btz), cysteine protease inhibitor, E64d, or DMSO (Mock) for one day. Total protein extracts from these plants were analyzed by immunoblotting using antibodies as indicated. Actin acted as a loading control. Typical immunoblotting results are shown (B). Band intensities were quantified and normalized to equivalent data for Actin (C). Data are means ± SEM from three biological replicates. In B, the arrowhead indicates full-length Toc159, and the hollow arrow indicates a truncated form of Toc159. Molecular weight markers (sizes in kD) are indicated to the right of the images. Asterisks in C indicate significance according to an unpaired two-tailed Student's *t*-test (*, significant at $P < 0.05$; **, significant at $P < 0.01$).

Figure 3. NBR1 is associated with autophagy at the envelope of chloroplasts.

A-C Presence of autophagosome in the chloroplast envelope. Arabidopsis protoplasts expressing free YFP and YFP-ATG8 (autophagosome marker) were analyzed by confocal microscopy. Corresponding chlorophyll autofluorescence images were employed to orientate the YFP signal in relation to the

chloroplasts. For eliminating interference from cytosolic signals, intact protoplasts (upper panels) were ruptured using 10-µm nylon mesh to isolate the chloroplasts. Retention of YFP signals in association with chloroplasts upon rupturing the cell (lower panels) clearly indicated that the YFP-ATG8 was associated with chloroplasts. Representative images are shown (A). In addition, whole protein samples of protoplasts and purified chloroplasts were analyzed by SDS-PAGE and immunoblotting, using antibodies against the YFP tag and Tic110 (a chloroplast marker). Typical immunoblotting results are shown (B). Band intensities were quantified and normalized to equivalent data for Tic110, to estimate protein abundance associated with chloroplasts (C).

D-E Identification of ATG8's interactors associated with chloroplasts. Chloroplasts were isolated as in B, and subjected to immunoprecipitation (IP) using anti-YFP magnetic beads. Total lysate and IP eluate samples were analyzed by immunoblotting using anti-YFP and anti-Tic40 (a TIC component used as a negative control) antibodies (D). The IP elution samples shown in D were analyzed by LC-MS/MS. This identified NBR1 and ~150 chloroplast proteins, which were selectively listed in E; a complete interactor dataset is provided in Dataset EV1. OEM, outer envelope membrane; IEM, inner envelope membrane.

F Localization of NBR1-YFP in the chloroplast envelope. Arabidopsis protoplasts (upper panels) expressing NBR1-YFP, and chloroplasts (lower panels) isolated from the protoplasts were analyzed by confocal microscopy, in procedures similar to A.

G, H Presence of NBR1-HA in chloroplast fraction. The protoplasts were isolated from four-week-old transgenic Arabidopsis plants stably expressing *p35S:NBR1-HA* (NBR1-HA) and *p35S:YFP-HA* (YFP-HA), followed by chloroplast purification, respectively. Protein samples of whole protoplasts and isolated chloroplasts of NBR1-HA and YFP-HA were then analyzed by SDS-PAGE and immunoblotting, using antibodies against the HA tag and Tic40. Typical immunoblotting results are shown (G). Band intensities were quantified and normalized to equivalent data for Tic40, to estimate protein abundance associated with chloroplasts (H). Data are means ± SEM from three biological replicates. Scale bars, 10 µm.

Figure 4. NBR1 targets TOC components for autophagy.

A NBR1 and TOC proteins colocalized at the chloroplast envelope of protoplasts. Arabidopsis protoplasts coexpressing the YFP-tagged chloroplast proteins and NBR1-CFP were analyzed by confocal microscopy following ConA treatment for four hours. Representative images are shown. Chlorophyll autofluorescence was used to determine the localization of the YFP fluorescence signals relative to the chloroplasts.

B Colocalization of NBR1 and TOC proteins in the central vacuole of Arabidopsis leaf cells. Eight-day-old transgenic Arabidopsis seedlings stably coexpressing *p35S:NBR1-mScarlet* and either *pToc33:YFP-Toc33* or *pToc75:YFP-Toc75* were treated with ConA for two days, and then analyzed by confocal microscopy. Accumulation of punctate bodies of overlapping fluorescence in the central vacuole are indicated by arrowheads.

C BiFC results showed interaction between NBR1 and TOC proteins. cYFP and nYFP refer to C-terminal YFP fragment and N-terminal YFP fragment, respectively. Reconstitution of YFP fluorescence was assessed after transient coexpression of the indicated pairs of fusion proteins. CDKA1 and OEP7 were used as negative controls for OEM and cytosolic proteins, respectively. Representative images are shown. Scale bars, 10 µm.

D The frequency of protoplasts showing a BiFC signal in C was quantified. All data are means ± SEM from three experiments.

E NBR1 coimmunoprecipitated with TOC proteins. Proteins were extracted from eight-day-old transgenic Arabidopsis seedlings stably expressing *p35S:NBR1-HA* or *p35S: NBR1-ΔUBA-HA*, or control seedlings only expressing *p35S:YFP-HA*, following UVB treatment for four hours. Obtained protein extract was analyzed by IP using anti-HA resin, and analyzed by immunoblotting of four endogenous proteins or HA-tagged proteins. Tic40 acted as negative controls. The asterisks indicate nonspecific cross-reacting bands. Arrow indicates the NBR1-HA band. The arrowhead indicates full-length Toc159 protein. Molecular weight markers (sizes in kD) are indicated to the right of the images.

Figure 5. NBR1 is involved in the autophagic degradation of TOC components during UVB stress.

A, B Phenotypes of seedlings under UVB stress. Briefly, eight-day-old WT, *atg7-2*, *nbr1-2* and NBR1-OX (overexpressor) seedlings grown under normal condition were subjected to UVB stress, with UVB treatment for 3 hours and recovery for 7 days. Representative plant images (A) and total chlorophyll content values (B) are shown; the latter provide a convenient metric for biomass. The chlorophyll values for the mutants and overexpressor plants were statistically significantly different from that for the WT (Student's *t* test; *, significant at $P < 0.05$; ***, significant at $P < 0.001$).

C, D TOC protein levels were regulated by autophagy in response to short-term UVB stress. Eight-day-old plants of indicated genotypes were subjected to UVB stress for the indicated times, and then analyzed by immunoblotting using 10 μg total protein extract loaded per lane (C, upper). Coomassie staining indicated that the treatments did not change the overall protein profile (C, lower). Band intensities were quantified and normalized to equivalent Actin data (D) Time 0 was taken as 100%. Unpaired two-tailed Student's *t*-tests revealed that the Toc159 protein level in *nbr1-2* ($P < 0.05$) and NBR1-OX ($P < 0.05$), the Toc75 protein level in *atg7-2* ($P < 0.05$), *nbr1-2* ($P < 0.01$), and NBR1-OX ($P < 0.05$), and the Toc33 protein level in *atg7-2* ($P < 0.05$), *nbr1-2* ($P < 0.01$), and NBR1-OX ($P < 0.05$), were significantly different from levels in the WT at the time of 1 d recovery from UVB stress.

E, F Toc159 was modified by both K48 and K63 ubiquitin linkage types. Eight-day-old WT plants were grown under normal growth condition (-), or subjected to UVB stress (+), with UVB treatment for four hours. The protein extract from the plants was analyzed by IP using native Toc159 antibody, or its preimmune serum as a negative control, and analyzed by immunoblotting using antibodies as indicated to the left of the images (E). Tic40 acted as a negative control. The asterisk indicates a truncated Toc159 form without A domain (Agne *et al*, 2010). Molecular weight markers (sizes in kD) are indicated to the right of the images. Please note that ubiquitin antibodies tend to produce stronger signals for hyper-ubiquitinated species than for hypo-ubiquitinated or mono-ubiquitinated species (based on the number of epitopes), which contrasts with the behaviour of the Toc159 antibody. Thus, the signals of the two antibodies are not expected to fully overlap. Poly-ubiquitinated Toc159 may not be detected by the Toc159 antibody due to the much lower abundance of these species compared with the mono-ubiquitinated or unmodified forms. This is why the poly-Ub K48 and K63 signals appear at higher molecular weight positions than the Toc159 signals. Relative Toc159 amounts modified by K48 or K63 ubiquitin linkage in plants with or without UVB stress were assessed by quantifying the smeary band intensity of the IP samples in α-K48 or α-K63 blots (F). All data are means ± SEM from three experiments.

Figure 6. NBR1 is involved in the autophagic degradation of TOC components during heat stress.

A Phenotypes of plants under heat stress (HS). Briefly, 25-day-old WT, *atg7-2*, *nbr1-2* and NBR1-OX (overexpressor) plants grown in soil under normal condition were subjected to heat stress, with 42°C treatment for 17 hours and recovery for 2 days. Representative plant images are shown.

B, C TOC protein levels were regulated by autophagy in response to short-term heat stress. Eight-day-old plants of indicated genotypes grown in vitro were subjected to short term heat stress, recovered for the indicated times, and then analyzed by immunoblotting using 10 μg total protein extract loaded per lane (B, upper). Coomassie staining indicated that the treatments did not change the overall protein profile (B, lower). Band intensities were quantified and normalized to equivalent Actin data (C). Time 0 was taken as 100%. Data are means ± SEM from three biological replicates. Unpaired two-tailed Student's *t*-tests revealed that the Toc159 protein level in *nbr1-2* ($P < 0.05$) and NBR1-OX ($P < 0.01$), and the Toc75 protein level in NBR1-OX ($P < 0.05$), were significantly different from levels in the WT at Time 12 h; and that the Toc159 protein level in *atg7-2* ($P < 0.001$), *nbr1-2* ($P < 0.01$), and NBR1-OX ($P < 0.001$), and the Toc75 protein level in *atg7-2* ($P < 0.01$), *nbr1-2* ($P < 0.01$), and NBR1-OX ($P < 0.01$), were significantly different from levels in the WT at Time 24 h.

Figure 7. Functional analysis of NBR1 reveals roles in chloroplast protein import and development.

A Analysis of protein import efficiency in vitro. Chloroplasts were isolated from 12-day-old WT, *nbr1-2* and NBR1-OX seedlings grown in vitro under normal condition, and were subjected to in vitro protein import assay by using 35S-labeled Rubisco small subunit (SSU) precursor protein as the import substrate, followed by corresponding quantification of the maturation of the radiolabeled precursor protein. A representative phosphor screen image is shown (upper left), and Coomassie staining of Rubisco large subunit (LSU) indicated equal loading (lower left); Times indicate minutes after the start of each import reaction. IVT, in vitro translation product used as a control. Together with similar images from two additional experiments, this was used to conduct the quantitative analysis shown (right); the amount of imported, mature protein in each sample was expressed as a percentage of that present at the final time point for the WT. Data are means ± SEM from three biological replicates.

B, C Analysis of protein import efficiency in vivo. The *35S:cpGFP* probe was analyzed in the eight-day-old WT, *ppi1*, *nbr1-2* and NBR1-OX backgrounds grown in vitro under normal condition (B) or UVB stress (C). UVB stress was conducted by UVB treatment for four hours followed by recovery for one day. The *ppi1* mutant lacks Toc33 and has constitutively reduced chloroplast protein import (Jarvis *et al.*, 1998). In each case, GFP signal recovery was measured following photobleaching, in hypocotyls of seedlings. Recovery was normalized using data from unbleached cells, and is expressed relative to the average normalized GFP signal across 4-5 cell fluorescence measurements taken three seconds apart before bleaching began. Data are means ± SEM from three biological replicates.

D-H Chloroplast development in WT, *nbr1-2* and NBR1-OX seedlings under UVB stress was studied. Cotyledons of eight-day-old plants grown in vitro under normal condition (D) or UVB stress (E) were analyzed by transmission electron microscopy, and representative images are shown. UVB stress was conducted in the same procedures as in C. In D and E, the upper images are at the same magnification (scale bar, 2 μm); and below these are high magnification (5×) images corresponding to the boxed regions above. These and similar micrographs of chloroplasts were used to determine chloroplast shape (F), the number of thylakoid lamellae per granum (G), and the number of starch granules per chloroplast (H) in each genotype, with or without UVB stress. Asterisks indicate significance according

to an unpaired two-tailed Student's *t*-test (*, significant at $P < 0.05$; ***, significant at $P < 0.001$; ****, significant at $P < 0.0001$). Values are means ± SEM from 30-50 chloroplasts.

Figure 8. NBR1 mutation suppresses the phenotype of plastid protein import mutant, *ppi1*.

A, B Phenotypes of two-week-old WT, *nbr1-2*, *ppi1* and *ppi1 nbr1-2* seedlings grown on soil. Representative plant images (A) and chlorophyll contents (B) are shown. The chlorophyll values for the *ppi1* and *ppi1 nbr1-2* plants were statistically significantly different (Student's *t* test; ****, significant at $P < 0.0001$). Values are means ± SEM from 20 plants.

C, D TOC protein accumulation was improved in *ppi1 nbr1-2* relative to *ppi1*. Two-week-old plants of indicated genotypes were subjected to immunoblotting analysis (C). Tic40 acts as a negative control, which does not change in response to the *ppi1* mutation. Numbers over the lanes indicate relative loading amounts of total protein extracts, and 100% = 10 μg. Band intensities were quantified and normalized to equivalent Tic110 data (D). The values of Toc159 protein abundances for the *ppi1* and *ppi1 nbr1-2* plants were statistically significantly different (Student's *t* test; ****, significant at $P < 0.0001$). Data are means ± SEM from three experiments.

E-G Chloroplast development in *ppi1* and *ppi1 nbr1-2* seedlings was studied. Cotyledons of two-week-old plants grown under normal condition as in A were analyzed by transmission electron microscopy, and representative images are shown (E). In E, the upper images are at the same magnification (scale bar, 1 μm); and below these are high magnification (3×) images corresponding to the boxed regions above. These and similar micrographs of chloroplasts were used to determine chloroplast size (F) and the number of thylakoid lamellae per granum (G) in each genotype. Asterisks indicate significance according to an unpaired two-tailed Student's *t*-test (****, significant at $P < 0.0001$). Values are means ± SEM from 30-40 chloroplasts.

Expanded View Figure Legends

Fig EV1. Subcellular localization analysis under control condition related to Figure 1.

Arabidopsis protoplasts expressing the YFP-tagged chloroplast proteins were analyzed by confocal microscopy, performed as described for Figure 1A except that the protoplasts were treated by dimethylsulphoxide (DMSO) for 4 h, as a control for the ConA treatment. Representative images are shown. Chlorophyll autofluorescence was used to determine the localization of the YFP fluorescence signals relative to the chloroplasts. Overlay of the YFP images on matching chlorophyll images (Merge) clearly indicated that the YFP signals of Toc33, Toc75 and Toc159 were localized around the periphery of the chloroplasts, a pattern which is indicative of envelope localization (same as the SP1 and FAX1 controls). In contrast with the controls, YFP fused TOC proteins also presented in the central vacuole of protoplasts treated with tonoplast ATPase inhibitor, ConA (Fig 1A), suggesting that TOC complex is degraded by autophagy. Scale bar, 10 μm.

Fig EV2. Quantification of YFP puncta in the vacuole related to Figure 2.

Hypocotyl cells of transgenic Arabidopsis seedlings stably expressing *pToc33:YFP-Toc33* or *pToc75:YFP-Toc75* in the wild-type and *atg7-2* mutant backgrounds were analyzed by confocal microscopy, performed as described for Figures 1D and 2A. The numbers of YFP puncta in the central vacuole per frame (4,000 μm^2 of hypocotyl section) were quantified. All values are means ± SEM from three experiments.

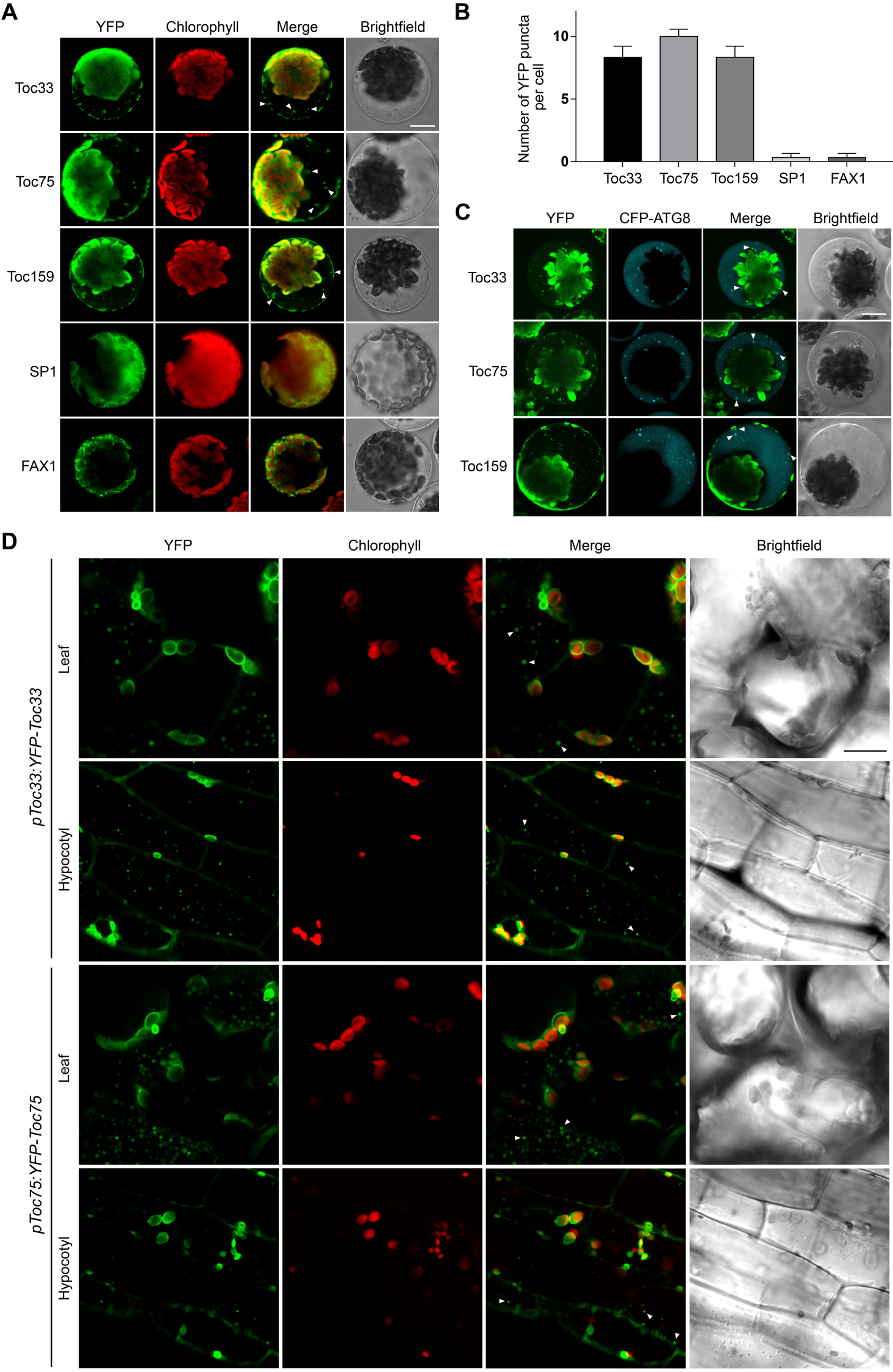
A
YFP
Chlorophyll
Merge
Brightfield
Toc33
Toc75
Toc159
SP1
FAX1
B
Number of YFP puncta per cell
10
5
0
Toc33
Toc75
Toc159
SP1
FAX1
C
YFP
CFP-ATG8
Merge
Brightfield
Toc33
Toc75
Toc159
D
YFP
Chlorophyll
Merge
Brightfield
pToc33:YFP-Toc33
Leaf
Hypocotyl
pToc75:YFP-Toc75
Leaf
Hypocotyl

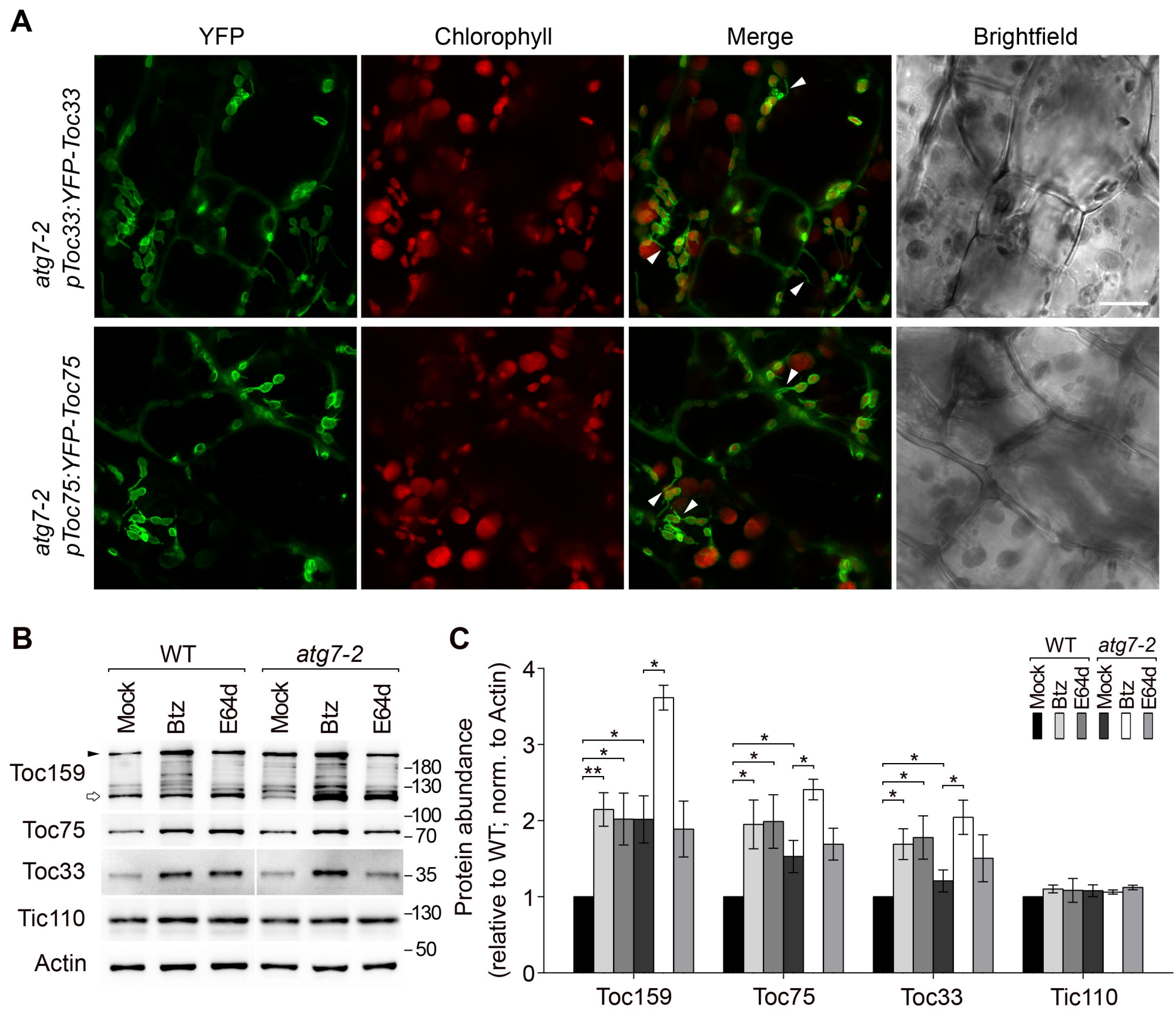
A
YFP
Chlorophyll
Merge
Brightfield
atg7-2
pToc33:YFP-Toc33
atg7-2
pToc75:YFP-Toc75
B
WT
atg7-2
Mock
Btz
E64d
Mock
Btz
E64d
Toc159
Toc75
Toc33
Tic110
Actin
180
130
100
70
35
130
50
C
WT
atg7-2
Mock
Btz
E64d
Mock
Btz
E64d
Protein abundance
(relative to WT; norm. to Actin)
0
1
2
3
4
Toc159
Toc75
Toc33
Tic110

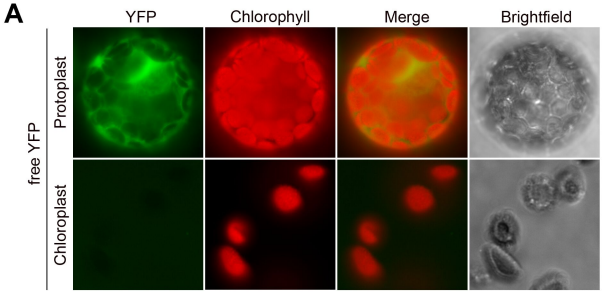

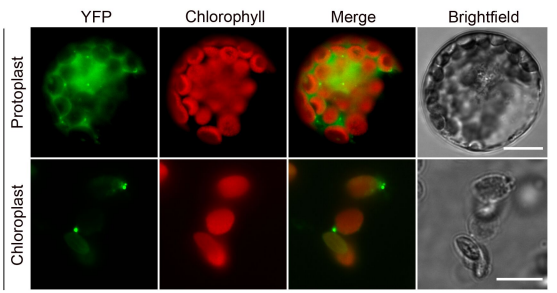

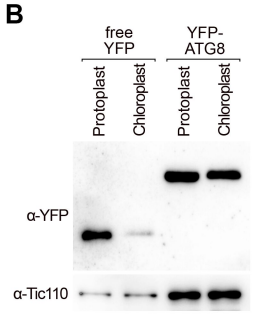

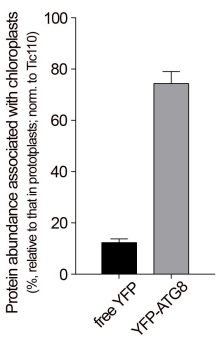

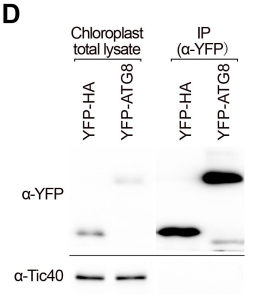

E

Protein name	AGI number	Biological function	Localization
NBR1	AT4G24690	Autophagy	Cytosol
Toc75	AT3G46740	Protein import	OEM
Toc33	AT1G02280	Protein import	OEM
OEP16	AT2G28900	Metabolite transport	OEM
Tic56	AT5G01590	Protein import	IEM
ClpC2	AT3G48870	Protein import	IEM
RCA	AT2G39730	Carbon reaction	Stroma
RPS4	ATCG00380	Protein translation	Stroma
rpoA	ATCG00740	RNA transcription	Stroma
PsaO	AT1G08380	PSI subunit	Thylakoid
PsbD	ATCG00270	PSII subunit	Thylakoid
LhcB1	AT1G29910	Light harvesting	Thylakoid

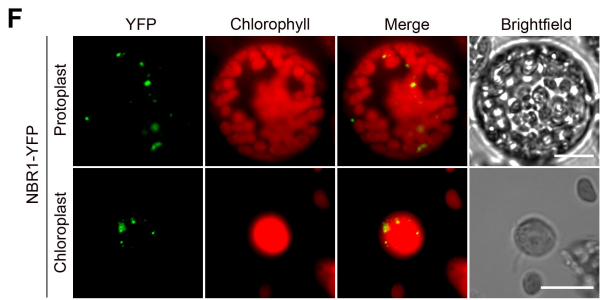

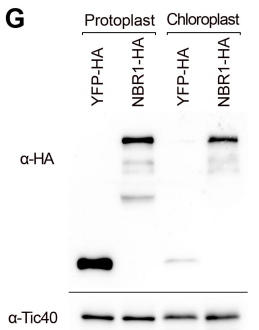

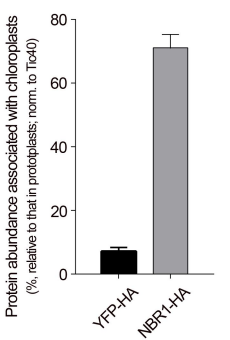

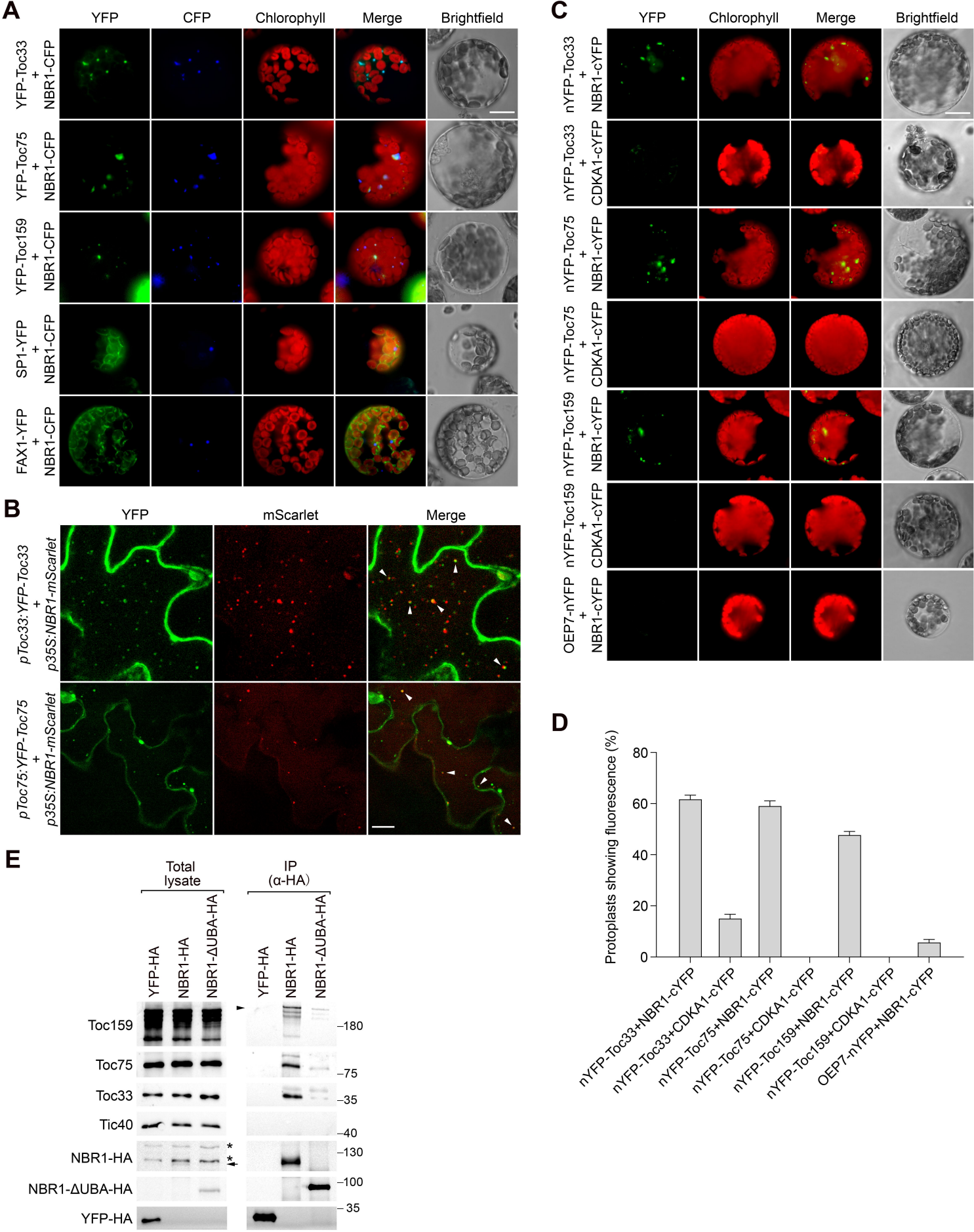
A
YFP
CFP
Chlorophyll
Merge
Brightfield
YFP-Toc33 + NBR1-CFP
YFP-Toc75 + NBR1-CFP
YFP-Toc159 + NBR1-CFP
SP1-YFP + NBR1-CFP
FAX1-YFP + NBR1-CFP
B
YFP
mScarlet
Merge
pToc33:YFP-Toc33 + p35S:NBR1-mScarlet
pToc75:YFP-Toc75 + p35S:NBR1-mScarlet
C
YFP
Chlorophyll
Merge
Brightfield
nYFP-Toc33 + NBR1-cYFP
nYFP-Toc33 + CDKA1-cYFP
nYFP-Toc75 + NBR1-cYFP
nYFP-Toc75 + CDKA1-cYFP
nYFP-Toc159 + NBR1-cYFP
nYFP-Toc159 + CDKA1-cYFP
OEP7-nYFP + NBR1-cYFP
D
Protoplasts showing fluorescence (%)
0
20
40
60
80
nYFP-Toc33+NBR1-cYFP
nYFP-Toc33+CDKA1-cYFP
nYFP-Toc75+NBR1-cYFP
nYFP-Toc75+CDKA1-cYFP
nYFP-Toc159+NBR1-cYFP
nYFP-Toc159+CDKA1-cYFP
OEP7-nYFP+NBR1-cYFP
E
Total lysate
IP (α-HA)
YFP-HA
NBR1-HA
NBR1-ΔUBA-HA
Toc159
Toc75
Toc33
Tic40
NBR1-HA
NBR1-ΔUBA-HA
YFP-HA
180
75
35
40
130
100
35

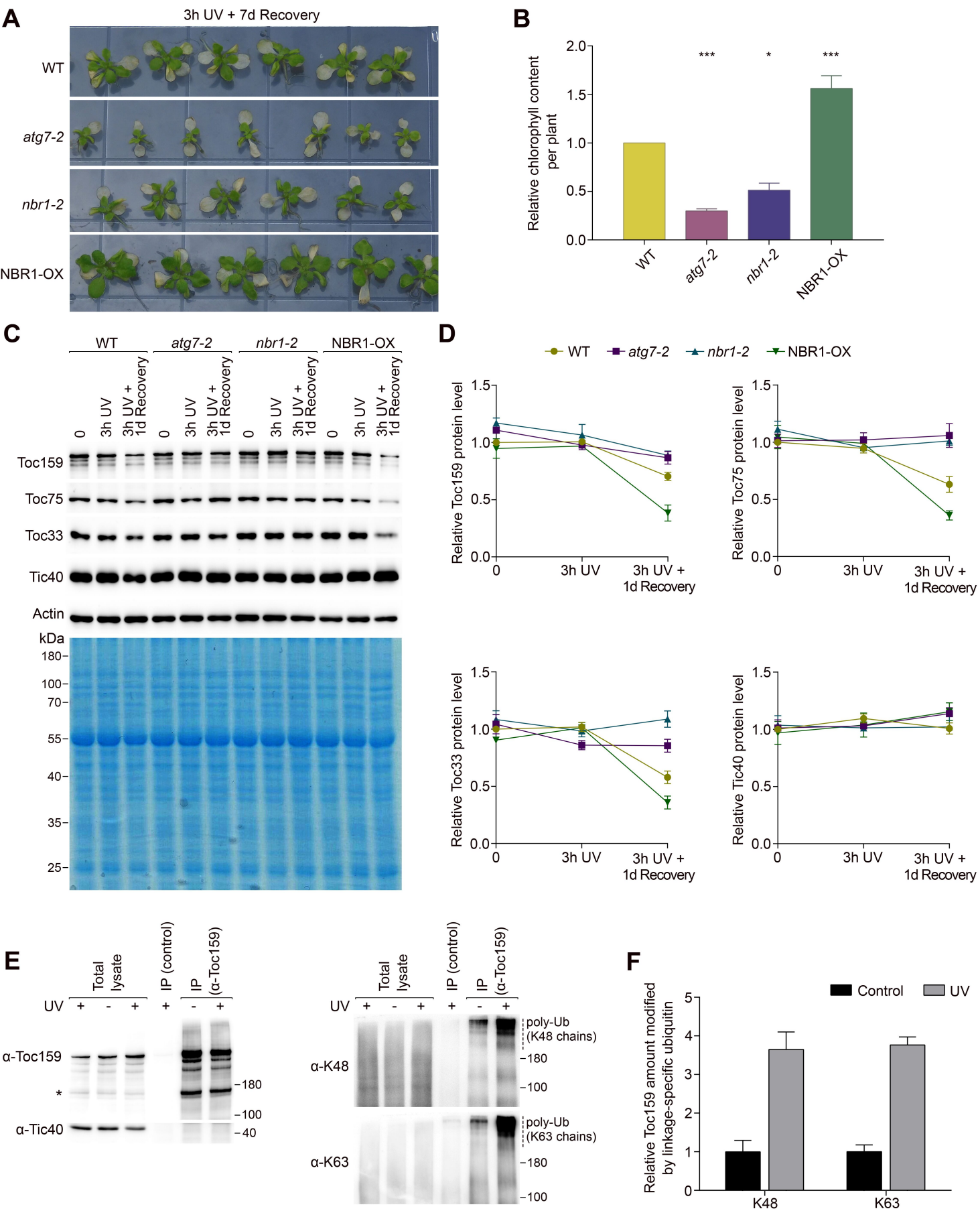
A
3h UV + 7d Recovery
WT
atg7-2
nbr1-2
NBR1-OX
B
Relative chlorophyll content per plant
2.0
1.5
1.0
0.5
0.0
***
*
***
WT
atg7-2
nbr1-2
NBR1-OX
C
WT
atg7-2
nbr1-2
NBR1-OX
0
3h UV
3h UV + 1d Recovery
Toc159
Toc75
Toc33
Tic40
Actin
kDa
180
100
70
55
40
35
25
D
WT
atg7-2
nbr1-2
NBR1-OX
Relative Toc159 protein level
Relative Toc75 protein level
Relative Toc33 protein level
Relative Tic40 protein level
1.5
1.0
0.5
0.0
0
3h UV
3h UV + 1d Recovery
E
Total lysate
IP (control)
IP (α-Toc159)
UV
+
-
α-Toc159
*
α-Tic40
180
100
40
α-K48
α-K63
poly-Ub (K48 chains)
poly-Ub (K63 chains)
F
Control
UV
Relative Toc159 amount modified by linkage-specific ubiquitin
5
4
3
2
1
0
K48
K63

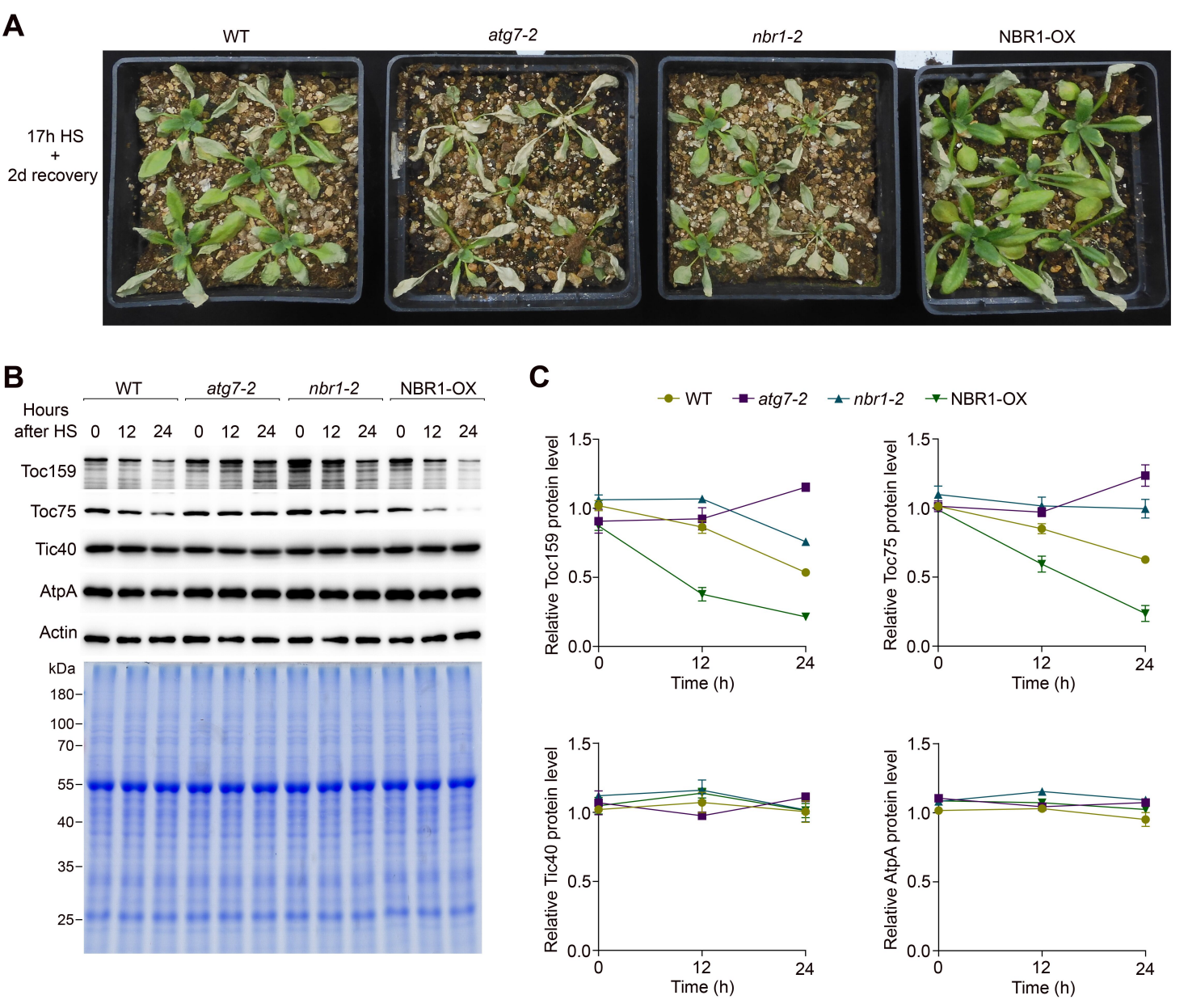
A
WT
atg7-2
nbr1-2
NBR1-OX
17h HS
+
2d recovery
B
WT
atg7-2
nbr1-2
NBR1-OX
Hours
after HS
0 12 24 0 12 24 0 12 24 0 12 24
Toc159
Toc75
Tic40
AtpA
Actin
kDa
180
100
70
55
40
35
25
C
WT
atg7-2
nbr1-2
NBR1-OX
Relative Toc159 protein level
Relative Toc75 protein level
Relative Tic40 protein level
Relative AtpA protein level
1.5
1.0
0.5
0.0
0
12
24
Time (h)

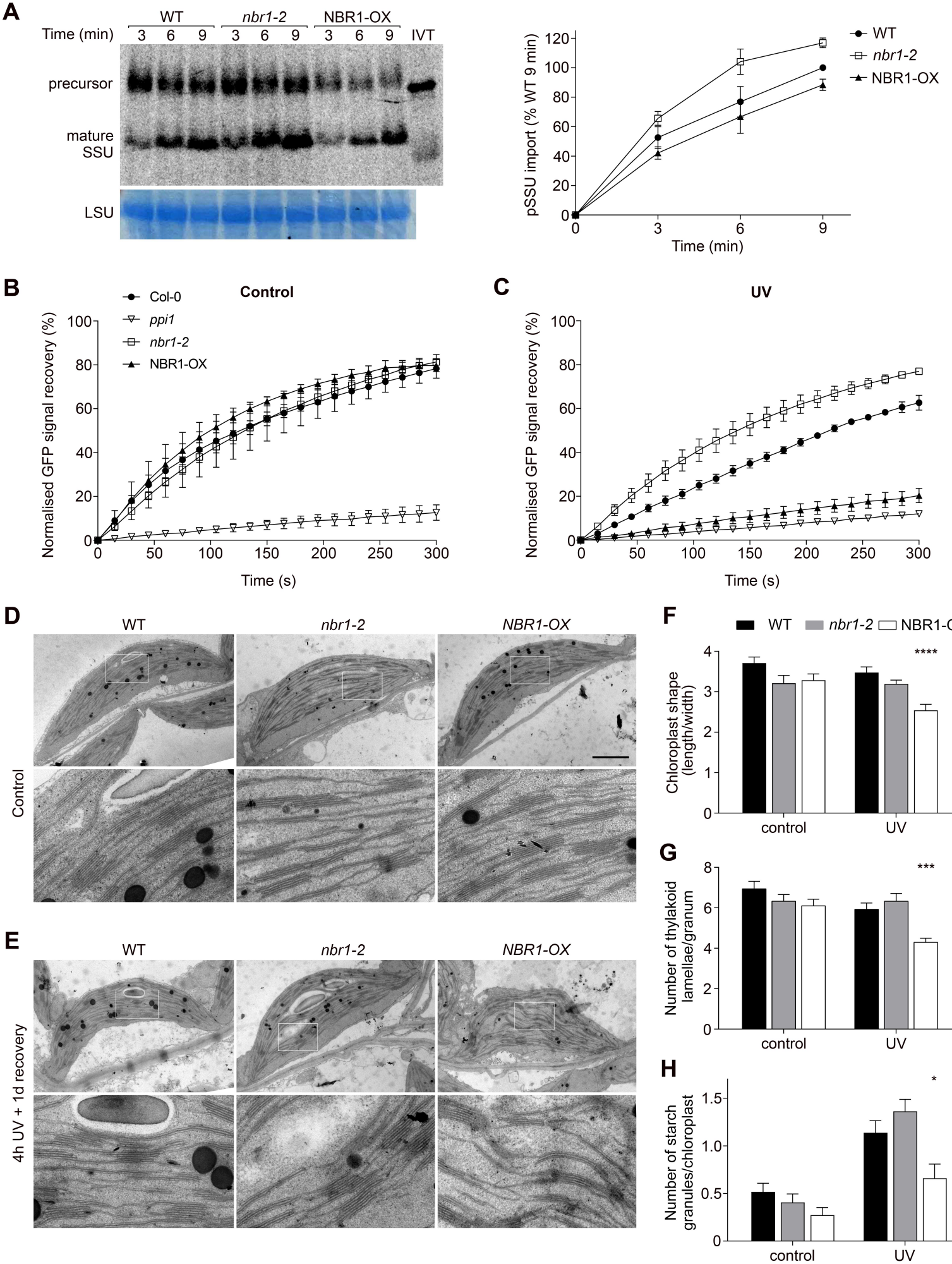
A
WT
nbr1-2
NBR1-OX
Time (min)
3 6 9 3 6 9 3 6 9 IVT
precursor
mature SSU
LSU
pSSU import (% WT 9 min)
Time (min)
WT
nbr1-2
NBR1-OX
B
Control
Col-0
ppi1
nbr1-2
NBR1-OX
Normalised GFP signal recovery (%)
Time (s)
C
UV
Normalised GFP signal recovery (%)
Time (s)
D
WT
nbr1-2
NBR1-OX
Control
E
WT
nbr1-2
NBR1-OX
4h UV + 1d recovery
F
WT
nbr1-2
NBR1-OX
Chloroplast shape (length/width)
****
control
UV
G
Number of thylakoid lamellae/granum
***
control
UV
H
Number of starch granules/chloroplast
*
control
UV

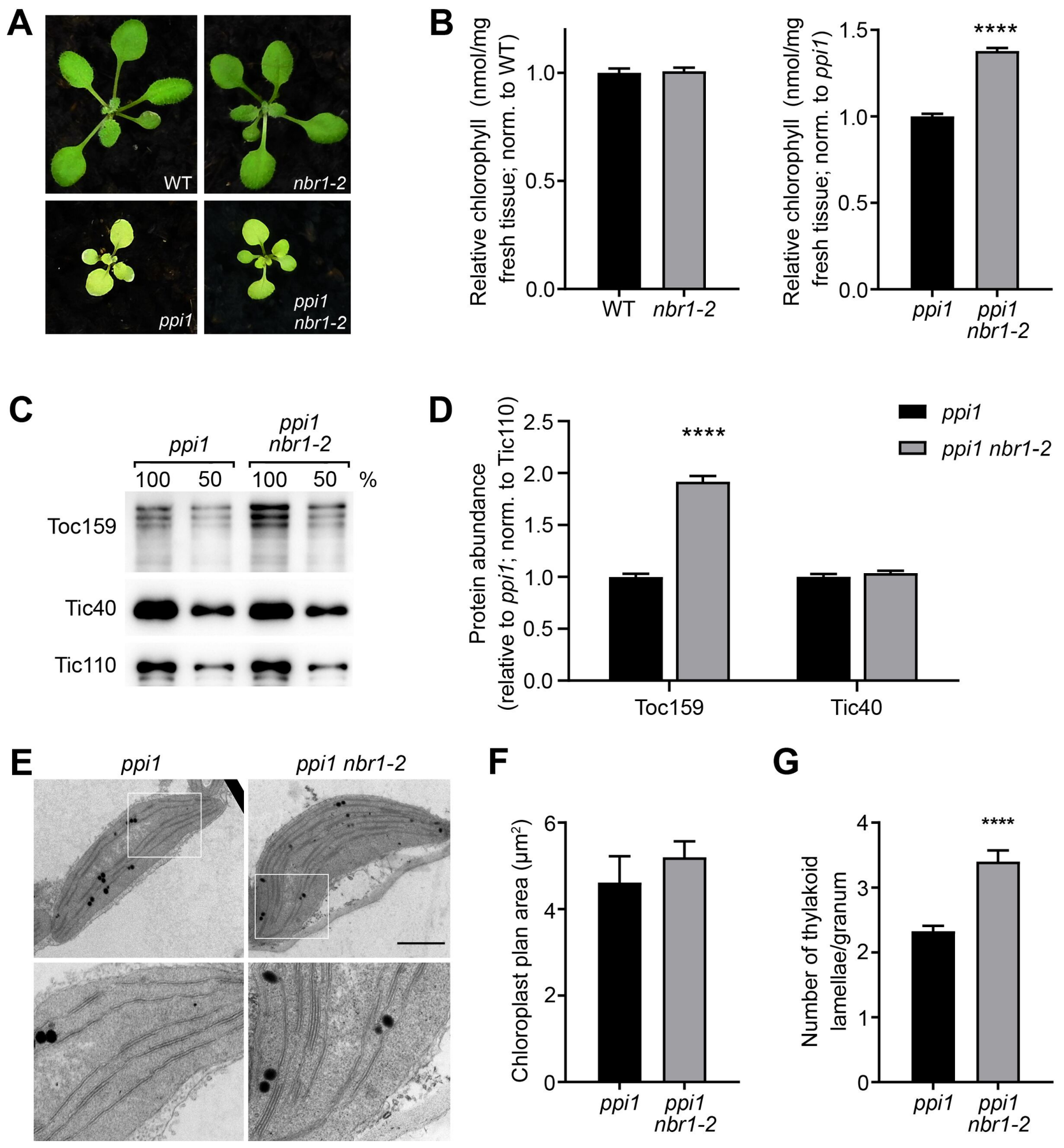
A
WT
nbr1-2
ppi1
ppi1
nbr1-2
B
Relative chlorophyll (nmol/mg fresh tissue; norm. to WT)
1.0
0.5
0.0
WT
nbr1-2
Relative chlorophyll (nmol/mg fresh tissue; norm. to ppi1)
1.5
1.0
0.5
0.0
****
ppi1
ppi1 nbr1-2
C
ppi1
ppi1 nbr1-2
100
50
100
50
%
Toc159
Tic40
Tic110
D
ppi1
ppi1 nbr1-2
Protein abundance (relative to ppi1; norm. to Tic110)
2.5
2.0
1.5
1.0
0.5
0.0
****
Toc159
Tic40
E
ppi1
ppi1 nbr1-2
F
Chloroplast plan area (µm²)
6
4
2
0
ppi1
ppi1 nbr1-2
G
Number of thylakoid lamellae/granum
4
3
2
1
0
****
ppi1
ppi1 nbr1-2

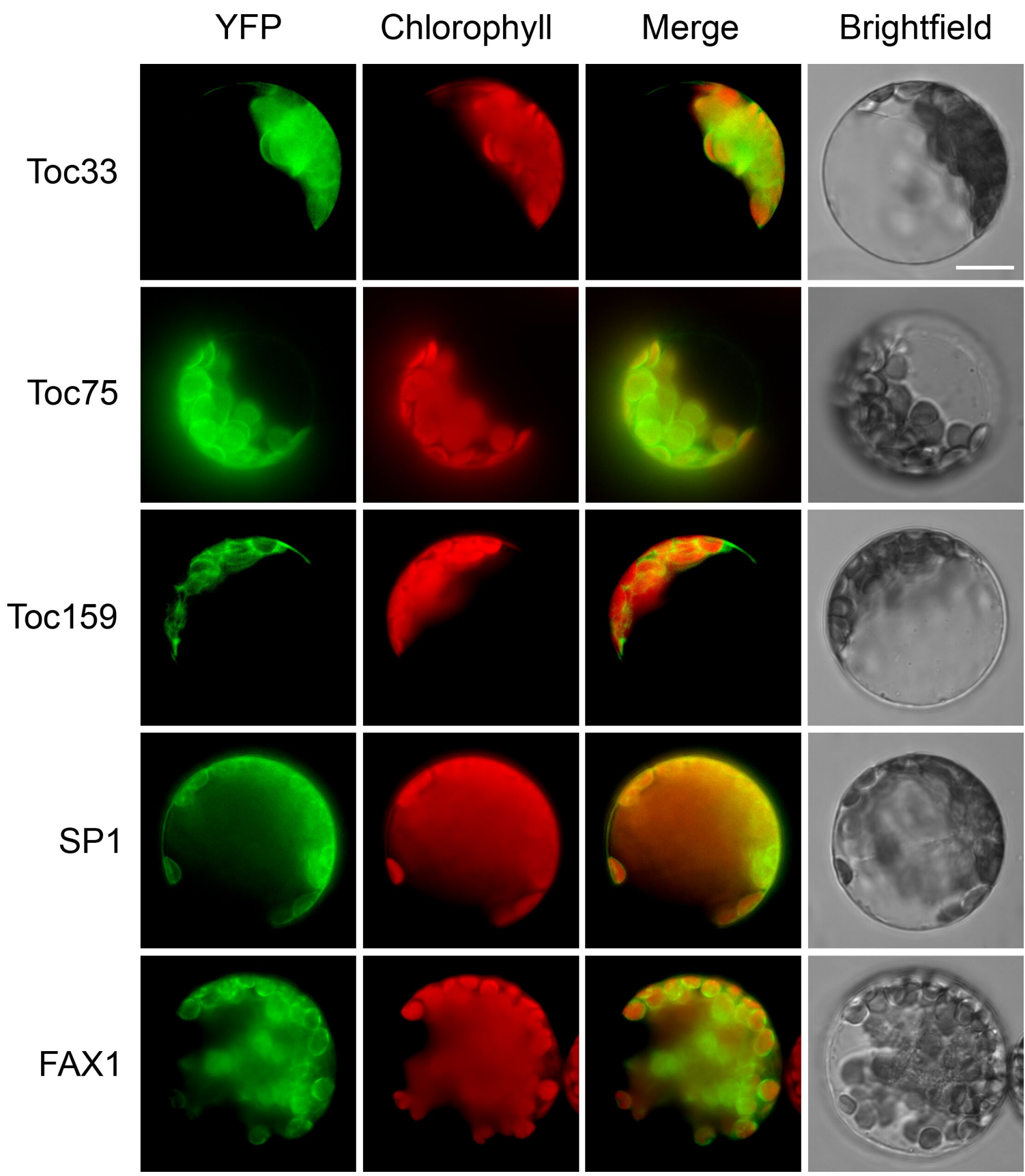
YFP
Chlorophyll
Merge
Brightfield
Toc33
Toc75
Toc159
SP1
FAX1

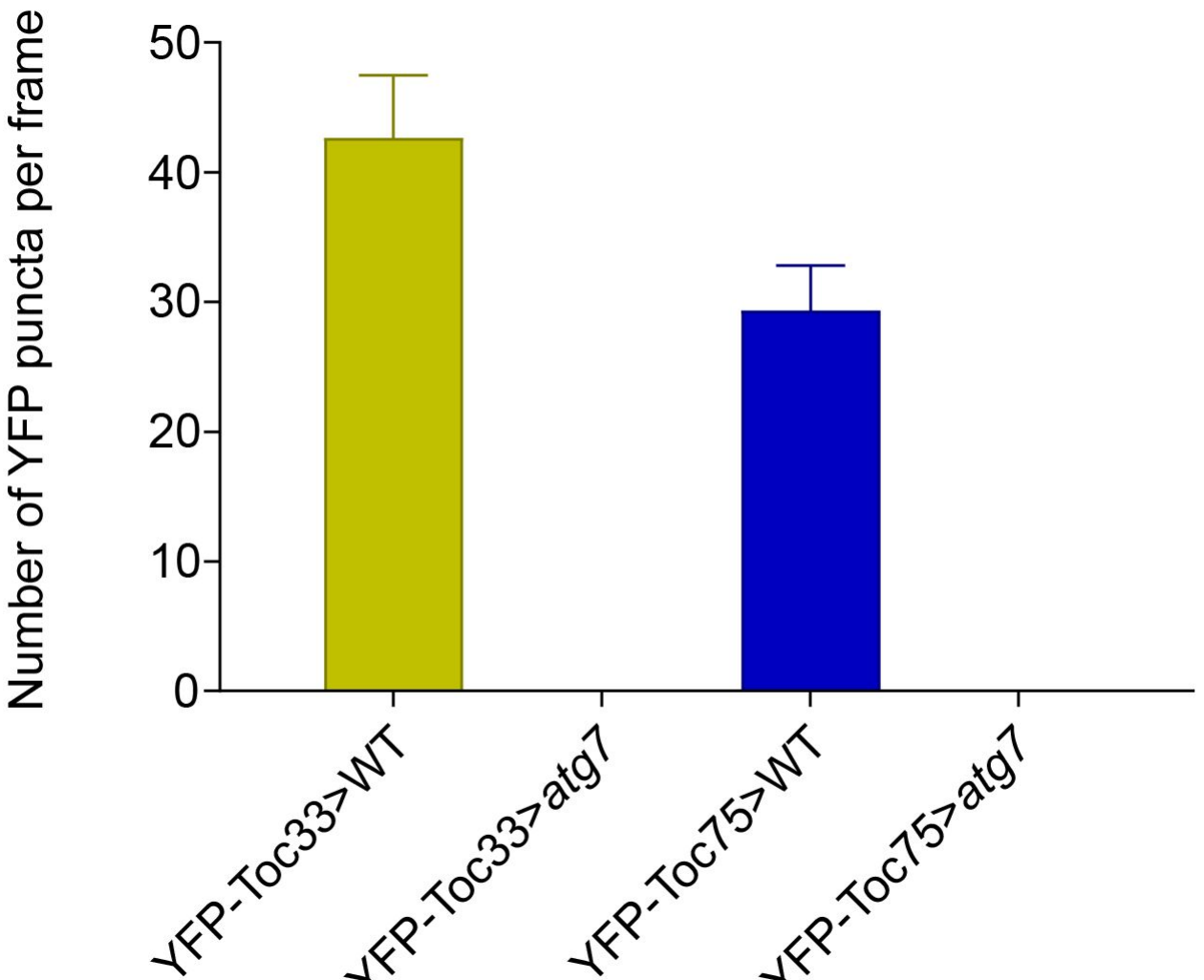
Number of YFP puncta per frame
50
40
30
20
10
0
YFP-Toc33>WT
YFP-Toc33>atg7
YFP-Toc75>WT
YFP-Toc75>atg7

Appendix for

Selective autophagy regulates chloroplast protein import and promotes plant stress tolerance

Chen Wan, Hui Zhang, Hongying Cheng, Robert G. Sowden, Wenjuan Cai, R. Paul Jarvis and Qihua Ling*

*Corresponding author: Qihua Ling, Email: qhling@cemps.ac.cn

Table of contents:

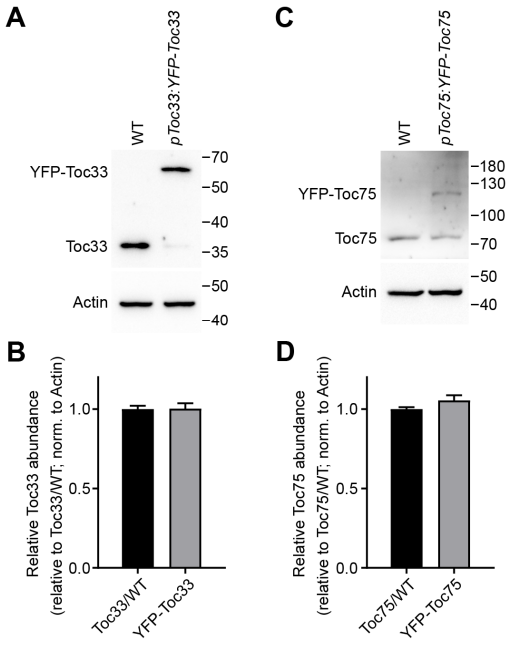

Appendix Figure S1. Levels of YFP-tagged TOC proteins in stable transgenic plants are similar to those of the endogenous proteins.

A-D Total proteins were extracted from eight-day-old transgenic Arabidopsis seedlings stably expressing *pToc33:YFP-Toc33* (A) and *pToc75:YFP-Toc75* (C), and wild-type (WT) control plants, and were analyzed by immunoblotting. Antibodies against Toc33 and Toc75 were used to detect both endogenous TOC proteins and YFP-tagged TOC proteins. Actin was used as a sample normalization control. Typical immunoblotting results are shown (A and C). Molecular weight markers (sizes in kD) are indicated to the right of the images. Band intensities for the TOC proteins were quantified and normalized to equivalent data for Actin (B and D). Data are means ± SEM from three biological replicates. The data show that the levels YFP-TOC fusion proteins are comparable to those of the endogenous proteins, and that the tagged proteins are not overexpressed.

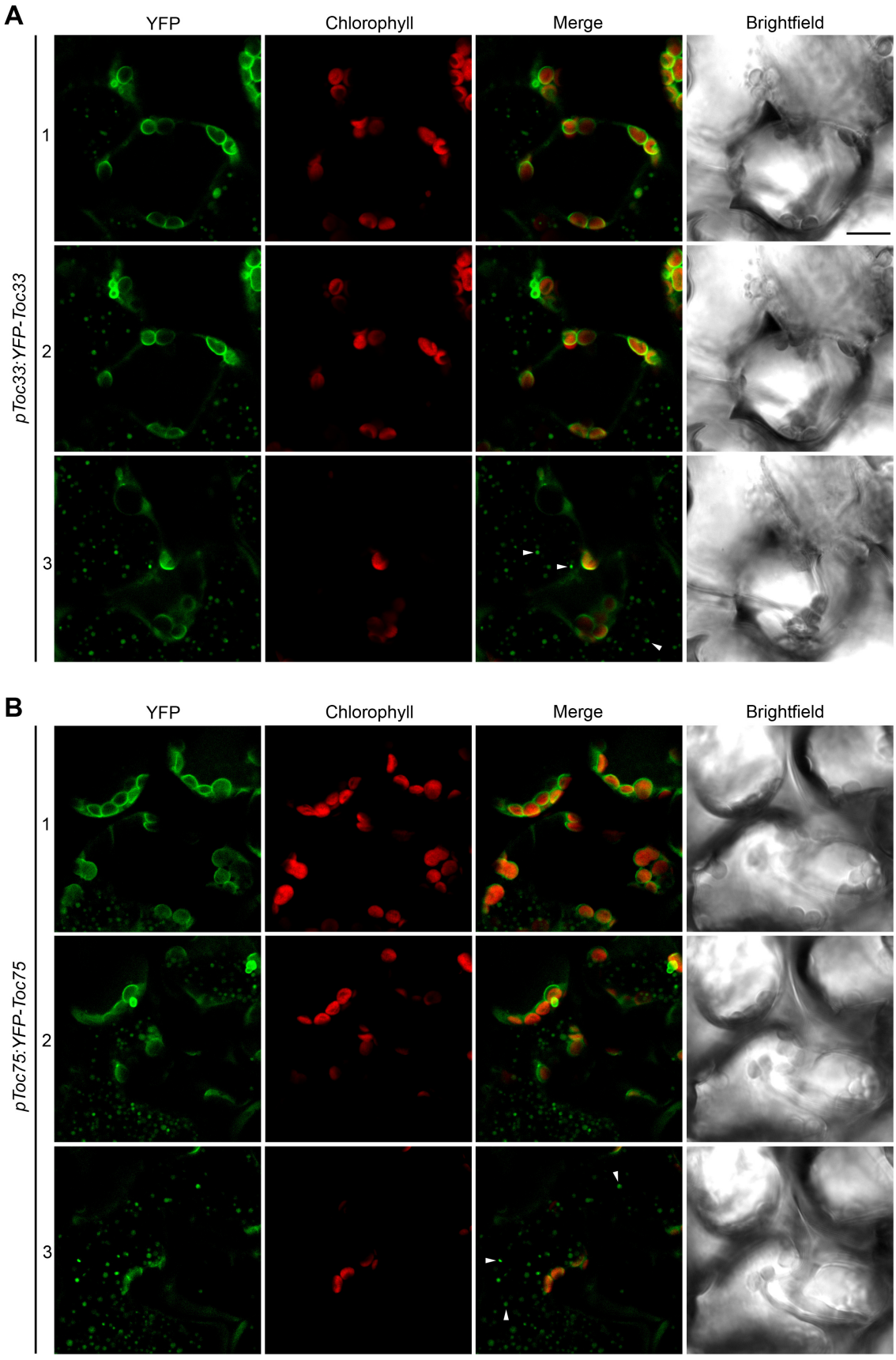
A
YFP
Chlorophyll
Merge
Brightfield
pToc33:YFP-Toc33
1
2
3
B
YFP
Chlorophyll
Merge
Brightfield
pToc75:YFP-Toc75
1
2
3

Appendix Figure S2. Analysis of the subcellular localization of YFP-tagged TOC proteins at different focal planes.

As described in Figure 1D, eight-day-old transgenic lines stably expressing *pToc33:YFP-Toc33* (A) or *pToc75:YFP-Toc75* (B) grown in vitro under normal conditions were treated with ConA for two days, before the YFP-fusion proteins in hypocotyl cells were analyzed by **s**pinning disk confocal microscopy. Chlorophyll autofluorescence was used to determine the localization of the YFP fluorescence signals relative to the chloroplasts. Accumulation of YFP puncta in the central vacuole is indicated by the arrowheads. Scale bar, 10 μm. Typical images for each sample with three different focal planes: panels with number 1 focus on chloroplast-associated YFP-TOC protein signals with the distributed envelope pattern; panels with number 3 focus on vacuolar YFP-TOC puncta; and panels with number 2 focus on planes in between numbers 1 and 3. Note that the vacuolar signals were generally much weaker than the chloroplast-associated signals, and thus were not easily observed in focal plane 1. In contrast, weaker chloroplast-associated YFP signals appear in focal plane 3 alongside stronger vacuolar signals. In Figure 1D, for simplicity, only focal plane **2** are shown.

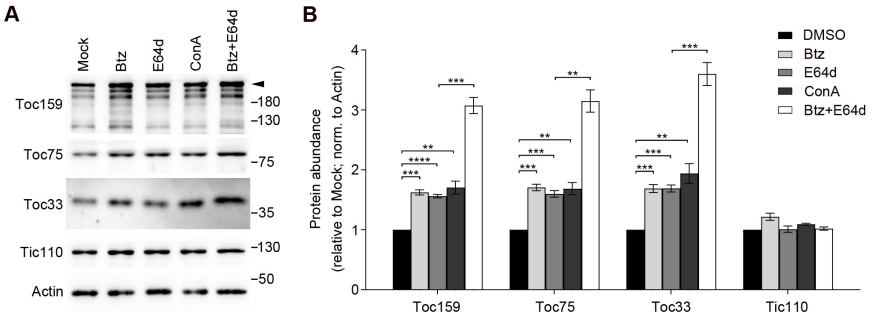

Appendix Figure S3. Further analysis of the effect of autophagy inhibition on TOC protein abundance.

Eight-day-old wild-type Arabidopsis plants were treated for one day with the proteasome inhibitor, bortezomib (Btz); the cysteine protease inhibitor, E64d; the tonoplast H^+-ATPase inhibitor, ConA; a combination of Btz and E64d, or DMSO solvent (Mock). Total protein extracts from these plants were analyzed by immunoblotting using antibodies as indicated. Actin acted as a loading control. Typical immunoblotting results are shown (A). The arrowhead indicates full-length Toc159. Molecular weight markers (sizes in kD) are indicated to the right of the images. Band intensities were quantified and normalized to equivalent data for Actin (B). Data are means ± SEM from three biological replicates. Asterisks in B indicate significance according to an unpaired two-tailed Student's *t*-test (**, significant at $P < 0.01$; ***, significant at $P < 0.001$; ****, significant at $P < 0.0001$).

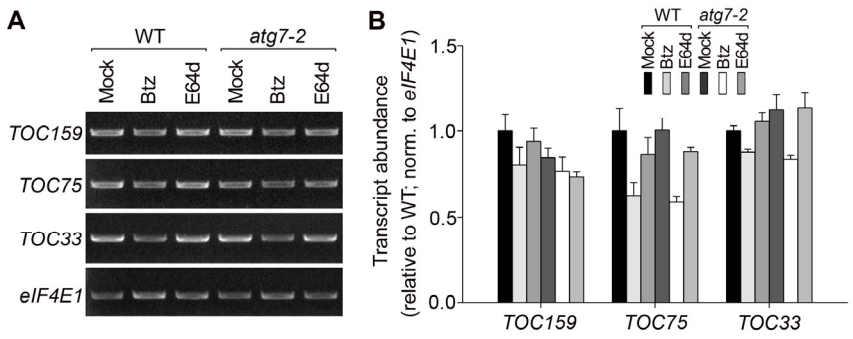

Appendix Figure S4. Accumulation of TOC proteins upon autophagy inhibition is not linked to elevated levels of the corresponding TOC mRNAs.

A Analysis of mRNA expression of TOC component genes when autophagy was suppressed. As described in Figure. 2, eight-day-old wild-type (WT) and *atg7-2* plants were treated respectively with proteasome inhibitor, bortezomib (Btz), cysteine protease inhibitor, E64d, or DMSO (Mock) for one day. Total RNA samples isolated from the treated plants were analyzed by semi-quantitative RT-PCR using gene-specific primers for *TOC159*, *TOC75-III*, *TOC33* and the reference gene *eIF4E1* (Table EV2). Amplifications employed a limited number of cycles to avoid saturation, and products were analyzed by agarose gel electrophoresis.

B The typical images shown in (A), together with similar images from two additional experiments, were used to conduct the quantitative analysis. Quantified band intensities were normalized to equivalent data for *eIF4E1*. Data are means ± SEM from three biological replicates. The results showed that mRNA levels of TOC component genes are not elevated either in autophagy mutant or plants treated with cysteine protease inhibitor, compared with control WT plants. This implies that the protein abundance changes in Fig 2 are mediated post-translationally.

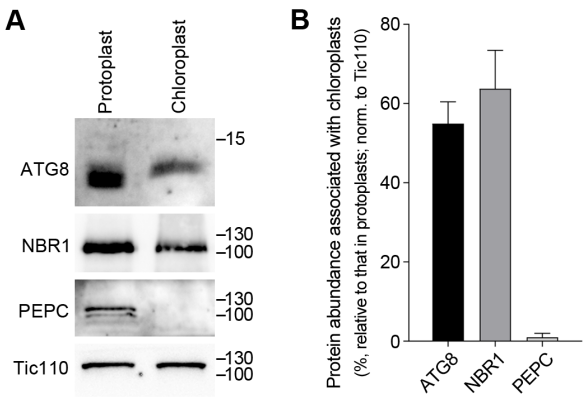

Appendix Figure S5. Endogenous ATG8 and NBR1 associate with chloroplasts.

Protoplasts were isolated from four-week-old wild-type Arabidopsis plants, followed by chloroplast purification, using procedures similar to those in Figure 3G. whole protoplast and isolated chloroplast protein samples were analysed by SDS-PAGE and immunoblotting (A), using antibodies against: ATG8, NBR1, PEPC (phosphoenolpyruvate carboxylase, a cytosolic marker), and Tic110 (a chloroplast marker). Molecular weight markers (sizes in kD) are indicated to the right of the images. Bands from the experiment shown, and those from two additional similar experiments, were quantified, and the values obtained for the indicated proteins were normalized using corresponding Tic110 data, to estimate protein abundance associated with chloroplasts (B). The presented data are means ± SEM (n = 3). Overall, the results show that substantial amounts of the endogenous ATG8 and NBR1 proteins interact with chloroplasts.

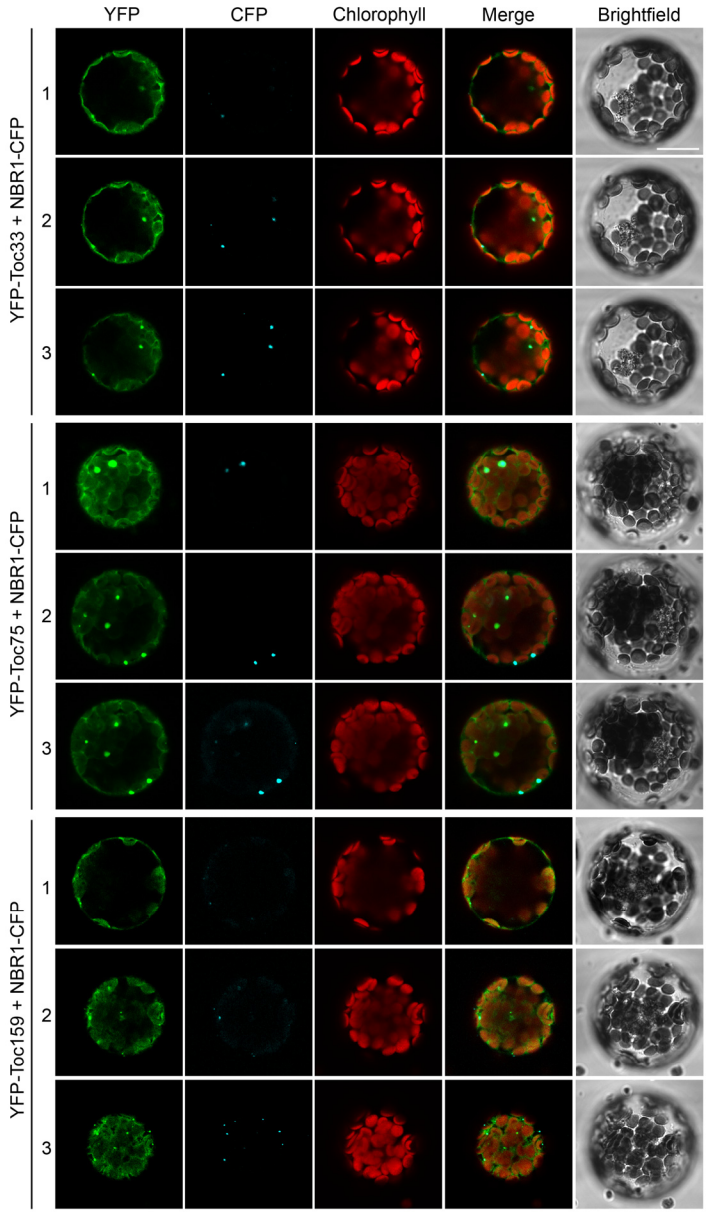

Appendix Figure S6. Analysis of the subcellular localization of tagged NBR1 and TOC protein by using different focal planes.

As described in Figure 4A, Arabidopsis protoplasts coexpressing the YFP-tagged TOC proteins and NBR1-CFP were analyzed by laser scanning confocal microscopy following ConA treatment for four hours. Chlorophyll autofluorescence was used to determine the localization of the YFP/CFP fluorescence signals relative to the chloroplasts. Scale bar, 10 µm. Typical images for each sample with three different focal planes: panels with number 1 focus on chloroplast-associated YFP-TOC protein signals with a distributed envelope pattern; panels with number 3 focus on the YFP-TOC/NBR1-CFP puncta; and panels with number 2 focus on planes in between numbers 1 and 3. The results show that the YFP-TOC protein signals were generally localized around the periphery of the chloroplasts in a pattern indicative of envelope localization. However, in some chloroplasts, YFP-TOC and NBR1-CFP colocalized in punctate structures adjacent to the

chloroplast envelope. In Figure 4A, for simplicity, only images focused on the NBR1-TOC puncta (similar to focal plane 3 here) are shown.

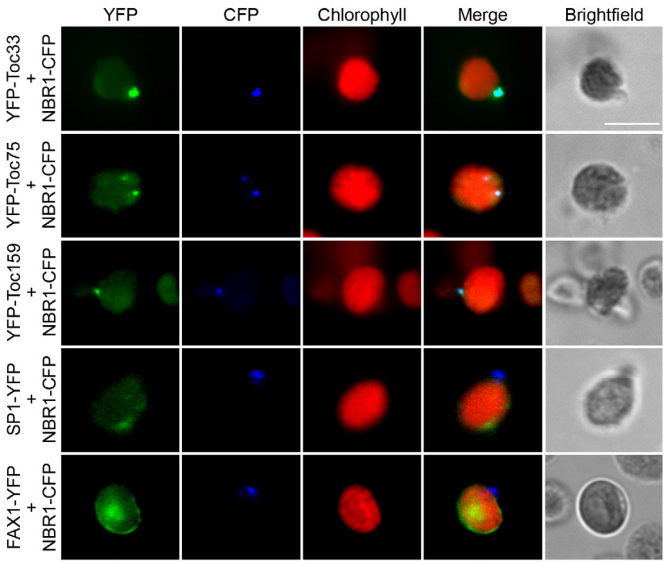

Appendix Figure S7. Colocalization of the YFP-TOC and NBR1-CFP proteins at the chloroplast envelope in isolated chloroplasts.

Arabidopsis protoplasts coexpressing the YFP-tagged TOC proteins and NBR1-CFP as described in Figure 4A were subjected to chloroplast isolation, in a procedure similar to Figure 3A. The YFP/CFP fluorescent signals in the isolated chloroplasts were analyzed by laser scanning confocal microscopy. Scale bars, 10 µm. Corresponding chlorophyll autofluorescence images were employed to orientate the YFP/CFP signals in relation to the chloroplasts. Retention of the YFP and CFP signals in association with isolated chloroplasts clearly indicated that the NBR1 and TOC proteins were colocalized in punctate structures at the periphery of the organelles, with patterns indicative of envelope localization.

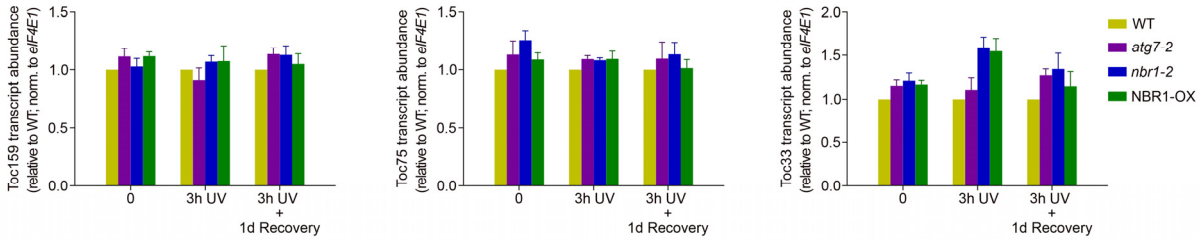

Appendix Figure S8. NBR1 does not obviously affect TOC component transcript levels under UVB stress.

As described in Figure 5C, eight-day-old WT, *atg7-2*, *nbr1-2* and NBR1-OX (overexpressor) seedlings grown under normal condition were subjected to UVB stress. Samples were respectively collected at three time points during the stress: immediately before the UVB treatment (0), after the UVB treatment for 3 h (3h UV), and after recovery for 1 d following the UVB treatment (3h UV + 1d Recovery). Total RNA samples isolated from the treated plants were analyzed by semi-quantitative RT-PCR using gene-specific primers for *TOC159*, *TOC75*, *TOC33* and the reference gene *eIF4E1*. Expression data for the *TOC* genes were normalized using equivalent data for *eIF4E1*. For each genotype tested, three biological replicates were analyzed, and the values shown are means ± SEM from three biological replicates. These results suggested that NBR1-mediated changes of TOC protein abundances under UV stress is not linked to changed levels of the corresponding TOC mRNAs.

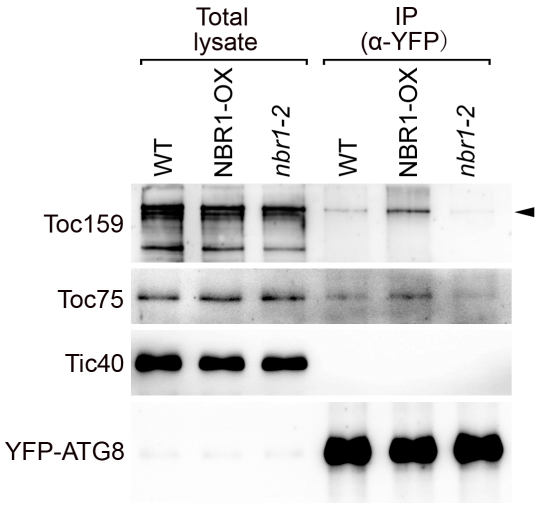

Appendix Figure S9. Interaction of ATG8 and TOC proteins depends on NBR1.

YFP-ATG8 construct was used to transfect protoplasts prepared from wild-type, NBR1-OX (overexpressor) and *nbr1-2* mutant plants. The cells were analysed by immunoprecipitation using anti-GFP magnetic beads. Total lysate (before immunoprecipitation was initiated) and the immunoprecipitated (IP) samples were then analysed by immunoblotting using antibodies against: the YFP tag, to verify the enrichment of YFP-ATG8; Toc159 and Toc75, to detect an ATG8-cargo interaction; and Tic40, to act as a negative control and confirm that the detected interactions are specific. Arrowhead indicates full-length Toc159 protein. The results suggest that NBR1 is responsible for recruiting ATG8 to its TOC protein cargos.

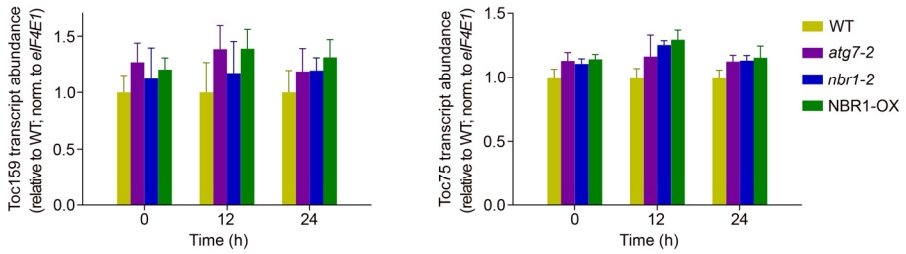

Appendix Figure S10. NBR1 does not obviously affect TOC component transcript levels under heat stress.

As described in Fig 6B, eight-day-old WT, *atg7-2*, *nbr1-2* and NBR1-OX (overexpressor) seedlings grown under normal condition were subjected to heat stress with 42°C treatment for 4 h. Samples were respectively collected at three time points after the heat treatment: immediately after the heat treatment (0), 12 hours after the heat treatment (12), and 24 hours after the heat treatment (24). Total RNA samples isolated from the treated plants were analyzed by semi-quantitative RT-PCR using gene-specific primers for *TOC159*, *TOC75* and the reference gene *eIF4E1*. Expression data for the *TOC* genes were normalized using equivalent data for *eIF4E1*. For each genotype tested, three biological replicates were analyzed, and the values shown are means ± SEM from three biological replicates. These results suggested that NBR1-mediated changes of TOC protein abundances under heat stress is not linked to changed levels of the corresponding TOC mRNAs.

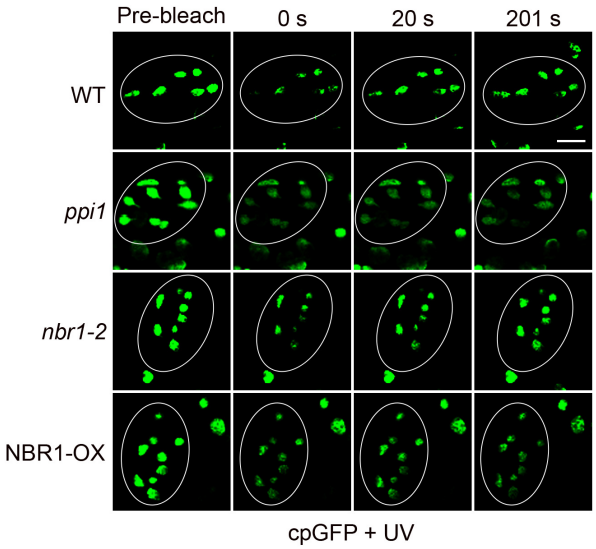

Appendix Figure S11. Confocal time-lapse series of cpGFP for analysis of protein import efficiency in vivo.

GFP tagged chloroplast precursor marker, *35S:cpGFP* was introduced into WT, *ppi1*, *nbr1-2* and NBR1-OX backgrounds by crossing. As reported previously, cpGFP typically shows chloroplast stromal localization. As described in Fig 7C, eight-day-old corresponding lines grown in vitro under normal condition were treated with UVB for 4 h followed by recovery for 1 d, before the cpGFP probe was analyzed by laser scanning confocal microscopy. In each case, images were initially recorded in hypocotyls of seedlings in a low intensity laser (Pre-bleach). Then the circled region containing a few chloroplasts were photobleached by intense laser light, reducing fluorescence from these chloroplasts (0 s), followed by time-resolved image recording of the samples (20 s and 201 s are shown). Unbleached chloroplasts serve as controls. Scale bar, 2 μm. The typical time-lapse series of cpGFP images are shown. And these images, together with other similar images from technical and biological replicates, were used for analysis of protein import efficiency in vivo in Fig 7C.

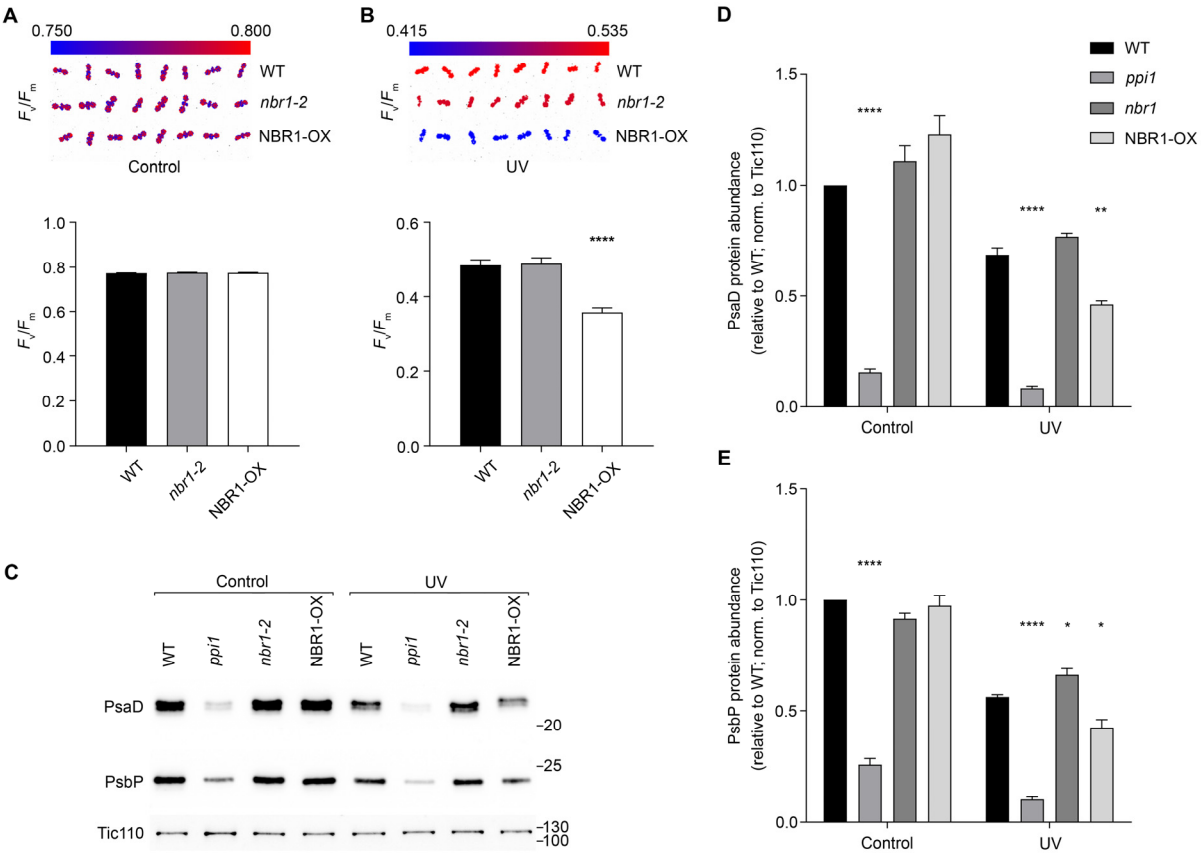

Appendix Figure S12. NBR1 suppresses photosynthesis under UVB stress conditions.

A-B Effect of *NBR1* on photosynthesis was assessed in plants grown under normal growth conditions (A) or UVB stress conditions (B). Eight-day-old WT, *nbr1-2* and NBR1-OX Arabidopsis seedlings grown in vitro under standard conditions were kept under the same conditions (Control), or were treated with UVB for 4 h followed by recovery for 1 d (UV), before photosynthetic performance (F_v/F_m) was analyzed. Typical leaf fluorescent images are shown in the upper panels of (A) and (B), with colour spectra representing the range of F_v/F_m values shown above the plant images. Average values were calculated using the images shown and other similar images, and are presented in the lower panels of (A) and (B). All values are means ± SEM of three experiments, and 8-10 seedlings were analyzed per genotype in each experiment.

C-E Effect of *NBR1* on the levels of photosynthetic proteins was assessed in WT, *ppi1*, *nbr1-2* and NBR1-OX Arabidopsis plants grown under normal growth conditions (control) or treated with UVB stress for 4 h followed by recovery for 3 d (UV). PsaD and PsbP are subunits of photosystem I and II, respectively, which are both imported into chloroplasts by the TOC complex. Total protein extracts from these plants were analyzed by immunoblotting using antibodies as indicated. Tic110 acted as a loading control. Typical immunoblotting results are shown (C). Molecular weight markers (sizes in kD) are indicated to the right of the images. Band intensities of PsaD (D) and PsbP (E) were quantified and normalized to equivalent data for Tic110. Data are means ± SEM from three biological replicates. Asterisks indicate significance relative to the WT, according to an unpaired two-tailed Student's *t*-test (*, significant at $P < 0.05$; **, significant at $P < 0.01$; ****, significant at $P < 0.0001$).

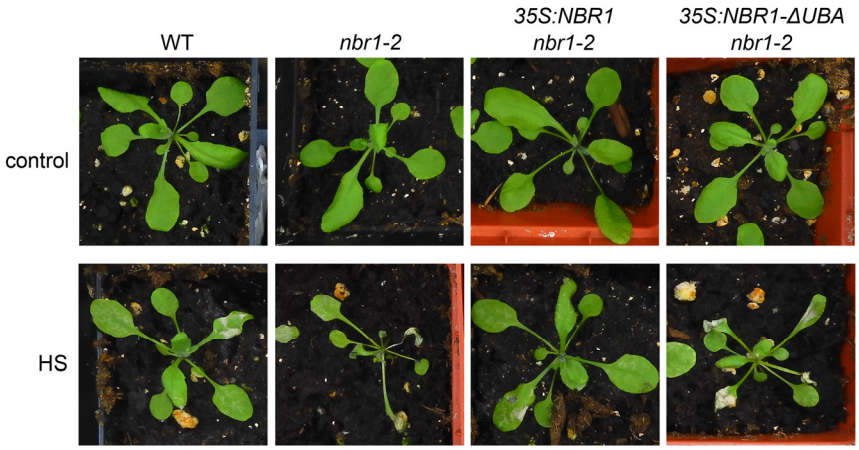

Appendix Figure S13. Ubiquitin binding domain, UBA, is essential for the function of NBR1.

The coding sequences (CDSs) of full length NBR1 or truncated NBR1 with the UBA domain deletion (ΔUBA) were respectively cloned downstream of the CaMV 35S promoter in the pH2GW7 binary vector. The resulting 35S:NBR1 and 35S:NBR1-ΔUBA binary constructs were then used to stably transform *nbr1-2* plants, respectively. Approximately 12 transformants were identified for each construct, and from these representative, single-locus lines were selected based on segregation of the T-DNA-borne antibiotic-resistance marker and *NBR1* gene expression. For phenotypic analysis, plants were grown under standard conditions on soil for 21 days followed by heat stress (HS) under 42°C for 10 h, and were then returned to the normal growth conditions (22°C) for 2 d before photography (lower panels). Non-heat-treated plants were used as controls (upper panels). Under heat stress, leaf necrosis was clearly apparent in both *nbr1-2* and *35S:NBR1-ΔUBA nbr1-2* plants, but not obvious in wild-type or *35S:NBR1 nbr1-2* plants, indicating that the *35S:NBR1-ΔUBA* construct failed to complement the *nbr1* mutation.

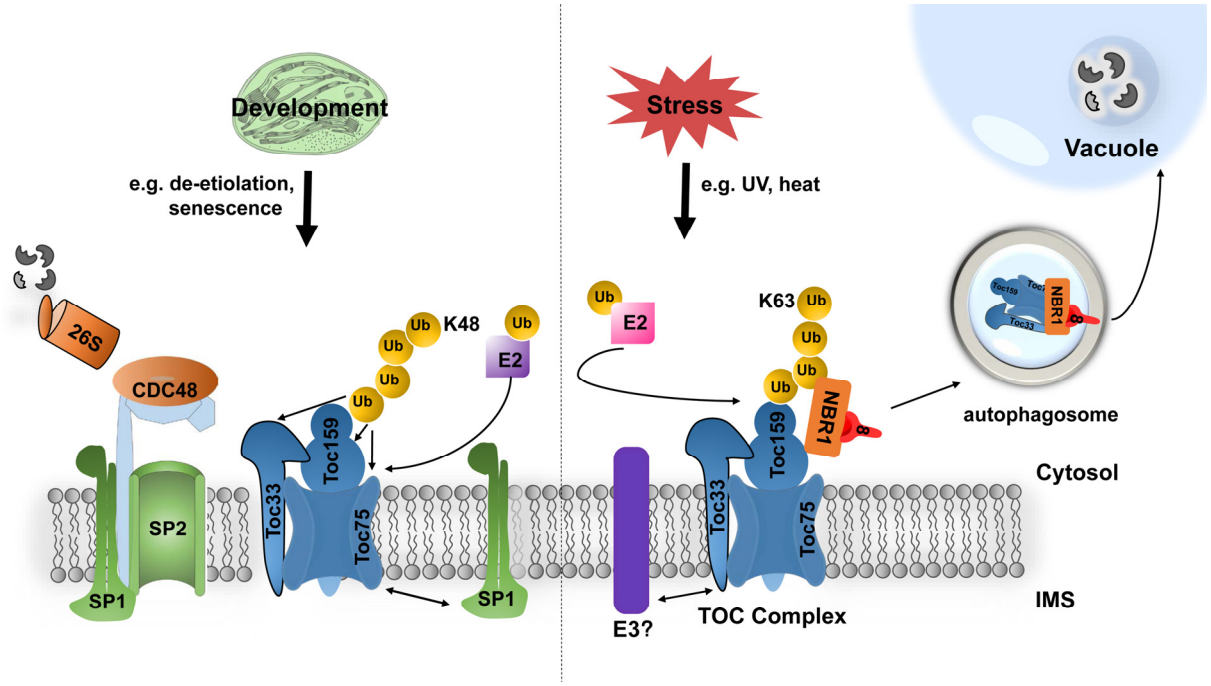

Appendix Figure S14. Model of ubiquitin-dependent selective TOC protein degradation.

The model presents two pathways of chloroplast proteolysis via protein ubiquitination, via autophagy and the UPS. These pathways act in the selective turnover of chloroplast TOC protein import machinery components for the regulation of plastid development and functions.

Right: Under certain stress condition, e.g., extreme light with high UVB levels or high temperature, photosynthesis tends to produce excessive reactive oxygen species (ROS) which can cause severe chloroplast damage. Under such circumstances, TOC components are poly-ubiquitinated through K63-based ubiquitin linkages, by an unknown chloroplast-associated E3 ligase, which can then be specifically recognized by the autophagy receptor NBR1. NBR1 facilitates docking of ubiquitinated TOC apparatus to the autophagosome through its interaction with ATG8, and the TOC protein cargos are subsequently delivered to the central vacuole for degradation. As a result, the import of new photosynthetic apparatus components is efficiently inhibited, which in turn suppresses photosynthetic activity and thus avoids overaccumulation of ROS and chloroplast damage.

Left: During developmental stages when plastids must change type, e.g., de-etiolation or fruit ripening, , or during stress, TOC components are degraded by the CHLORAD system. The proteins are poly-ubiquitinated through K48-based ubiquitin linkages, by the chloroplast-localized E3 ligase SP1, and then retrotranslocated to the cytosol via the SP2 channel and the CDC48 chaperone motor, and finally degraded by the 26S proteasome. This enables reorganization of the protein import machinery to help the plastid adapt to developmental transitions or environmental conditions.